Canadian Science Publishing | Canadian Journal of Earth Sciences

Geochemical characteristics of Late Jurassic-Early Cretaceous platform carbonates in Hazine Mağara, Gümüşhane (NE Turkey): Implications for dolomitization and recrystallization

Journal:	*Canadian Journal of Earth Sciences*
Manuscript ID	cjes-2018-0168.R3
Manuscript Type:	Article
Date Submitted by the Author:	06-Nov-2018
Complete List of Authors:	Özyurt, Merve; Karadeniz Teknik Universitesi, Geology Engineering Department; University of Windsor, Department of Earth and Environmental Sciences Kırmacı, M. Ziya; Karadeniz Teknik Universitesi Al-Aasm, Ihsan; Dept of Earth Sciences,
Keyword:	Geochemistry, Carbonate diagenesis, Dolomitization, Recrystallization, NE Turkey
Is the invited manuscript for consideration in a Special Issue? :	Advances in low temperature geochemistry diagenesis seawater and climate: A tribute to Jan Veizer

SCHOLARONE™
Manuscripts

Geochemical characteristics of Upper Jurassic-Lower Cretaceous platform carbonates in Hazine Mağara, Gümüşhane (NE Turkey): Implications for dolomitization and recrystallization

Merve Özyurt[1,2], M. Ziya Kirmaci[1], and Ihsan. S. Al-Aasm[2]

[1]Department of Geological Engineering, Karadeniz Technical University, 61080, Trabzon, Turkey; merveyildiz@ktu.edu.tr, kirmaci@ktu.edu.tr.

[2]Department of Earth and Environmental Sciences, University of Windsor, Windsor, ON N9B 3P4, Canada; alaasm@uwindsor.ca.

Corresponding author: Merve Özyurt (email: merveyildiz@ktu.edu.tr, ozyurt@uwindsor.ca).

Draft

Abstract: Upper Jurassic-Lower Cretaceous Berdiga Formation of the Eastern Pontide, Turkey represents a carbonate platform succession comprised of pervasively dolomitized intra-shelf to deep shelf facies. In this area, polymetallic deposits occur as veins and lenses within the Berdiga Formation in close proximity to its upper contact with the overlying formation. Three different types of replacive dolomites occur in the formation: 1) microcrystalline dolomite (Md Dolomite); 2) fabric-preserving dolomite (Fpd Dolomite), and 3) fabric-destructive dolomite (Fdd Dolomie). Replacive dolomites are Ca-rich and nonstoichiometric ($Ca_{56-58}Mg_{42-44}$) and are characterized by a pronounced negative shift in oxygen (–11.38 to –4.05 ‰V-PDB), $\delta^{13}C$ values of 0.69 to 3.13 ‰V-PDB, a radiogenic $^{87}Sr/^{86}Sr$ ratios (0.70753 to 0.70884), extremely high Fe (2727-21053 ppm) and Mn (1548-27726 ppm) contents. All dolomite samples have low Y/Ho ratios (23 to 40) and they also contain highly variable contents of REE (7 to 41). Rare earth elements (REE) patterns of dolomites normalized to PAAS show distinct positive Eu anomaly (1.3 to 2.1) and slightly flattened Ce anomalies (0.8 to 1.1). Integration of petrographic and geochemical studies reveal the history of a variety of diagenetic processes

highly affected by hydrothermal alteration, which include dolomitization, recrystallization, dissolution, silicification and pyrite mineralization associated with the emplacement of the polymetallic mineralization.

Keywords: Geochemistry; carbonate diagenesis; dolomitization; recrystallization; NE Turkey.

Draft

Introduction

Dolomite [$CaMg(CO_3)_2$] is a common diagenetic mineral. Dolomite formation and its alteration is still a matter of debate (e.g. Budd 1997; Al-Aasm et al. 2000; Warren 2000; Machel 2004; Gregg et al. 2015). A number of models have been proposed in order to understand the nature of paleofluid flow and its driving mechanisms of the formation of extensive dolomitization during shallow to deep burial conditions (Morrow 1998; Warren, 2000; Al-Aasm 2003; Congwei et al. 2013). In recent years, massive dolomite bodies and their diagenetic alterations due to hydrothermal fluids have been increasingly documented because of their potential as hydrocarbon reservoirs and economic base-metals ore-deposits (e.g., Leach and Sangster 1993; Wendte et al. 1998; Warren 2000; Muchez et al. 2005; Davies and Smith 2006; Morrow 2014; Jiang et al. 2016; Navarro-Ciurana 2016). However, many researchers proposed that it is very difficult to reveal the origin of dolomitization, because the massive dolomite bodies are generally affected by chemical alteration due to hydrothermal fluid flow which is affected by different tectonic event, magmatic generation and related polymetallic mineralizations during progressive burial history (e.g., Al-Aasm 2000; Al-Aasm and Packard 2000; Garven 1985; Muchez et al. 2000; Martín-Martín 2015; Adam and Al-Aasm 2017; Navarro-Ciurana 2016). Therefore, nowadays, besides traditional petrographic and geochemical analyses (e.g., Sr, Na, Fe, Mn, ^{13}C, ^{18}O, and $^{87}Sr/^{86}Sr$), rare earth elements (REEs) of dolomite have been extensively applied to provide an important insights into tracing the origins of dolomitization and hydrothermal alterations in dolomites (e.g., Banner et al. 1988; Qing and Mountjoy 1994; Wendte et al. 1998; Azomani et al. 2013). However, various questions still remain debated concerning REE signatures of dolomite, because these signatures can be significantly altered by meteoric water and hydrothermal fluids during the diagenetic evolution (Murray et al. 1991; Webb and Kamber 2011; Shields and Stille 2001; Nothdurft et al. 2004; Webb et al. 2009). Nowadays numerous studies have been focused on

Draft

the origin of dolomite using its REE signature (Wang et al. 2014; Liu et al. 2017; Yang et al. 2018). These studies suggest that both contents of REE and their distinct patterns can be used as geochemical tools to provide a better understanding of hydrothermal alteration and evolution of dolomites (Hecht et al., 1999; Bau and Alexander 2006; Yang et al. 2018).

Large-scale, massive dolomite bodies are well preserved in the Eastern Pontides (NE Turkey), which is known as one of the best examples of the metallogenic provinces in on the Alpine-Himalayan belt. These dolomite bodies are hosted in the Upper Jurassic-Lower Cretaceous Berdiga Formation composed of platform carbonates. In this region, Berdiga Formation was investigated by many researchers in terms of its stratigraphic, lithologic and structural attributes (e.g. Taslı 1991; Kırmacı 1992; Koch et al. 2008 and many others), but little efforts have been made to contribute to the understanding of the origin of dolomitization (Kırmacı et al. 2018). Moreover, massive dolomite bodies of Berdiga Formation hosts important economic mineralizations (Pb-Zn-Cu-Au-Ag) in Hazine Mağara area, which comprises one of the typical exposures of the succession in the southern part of Eastern Pontides (Akçay et al. 2011). However, there have not been attempts for a better understanding of the effect of hydrothermal fluids on dolomites and the relationship with Pb-Zn-Cu-Au-Ag occurrences. Therefore, the study area is an ideal location to understand not only the origin of dolomite but also the later influence of hydrothermal fluids associated with poly-metallic mineralizations. This will be accomplished via traditional petrographic and geochemical analyses combined with rare earth elements signatures. Hence, in the present study, we focus on the massive dolomite bodies in Hazine Mağara area with the main objectives:

(1) To decipher the diagenetic evolution of the formation and origin of dolomite; and (2) to provide a better understanding of the hydrothermal alteration associated with emplacement of the polymetallic mineralization on dolomites.

Draft

Regional Geological Framework

Sakarya Zone, which geographically corresponds to the northern part of Turkey, is bordered by the Black Sea to the north and by the İzmir-Ankara-Erzincan suture to the south (e.g., Okay and Tüysüz 1999). The eastern part of the Sakarya Zone is generally called as Eastern Pontides (Fig. 1). The Eastern Pontides has experienced Alp-Himalayan tectono-magmatic evolution and represents one of the most important metallogenic provinces in the Alpine-Himalayan Orogenic Belt system and (e.g. Ketin 1966). The studied massive dolomite bodies are well exposed in the southern part of the Eastern Pontides (Fig. 1). Stratigraphically, the Hercynian basement of the area is composed of pre-Carboniferous high-degree metamorphic complex and Permo-Carboniferous granitoid intrusions (Okay and Şahintürk 1997). Lower-Middle Jurassic volcano-sedimentary series are considered as rift sediments (Şenköy Formation; 2000 m thick) unconformably overlie the Hercynian basement. Upper Jurassic-Lower Cretaceous has witnessed relatively stable tectonic regime in the Eastern Pontides, on which is located at the passive continental margin of the northern branch of Neotethys (Görür 1988; Okay and Şahintürk 1997). In addition to the stable tectonic regime, equatorial-subequatorial paleoclimate conditions facilitated the deposition of Upper Jurassic-Lower Cretaceous carbonates (Berdiga Formation). The Upper Jurassic-Lower Cretaceous carbonates, which overlain generally conformably the rift-related volcano-sedimentary sequence, have been studied by numerous authors (e.g. Kırmacı 1992; Kırmacı et al. 1996; Koch et al. 2008; Taslı et al. 2000). The carbonates were described as mainly composed of platform carbonates showing varying lithofacies; changing from supratidal to slope both laterally and vertically (Taslı 1991; Kırmacı 1992; Kırmacı et al. 1996; Koch et al. 2008). In addition, in many recent studies researchers show that vertical movement of the syn-sedimentary extensional tectonic regime might probably caused the progressive deepening of

Draft

the environment, so the inner platform environment evolved into an outer platform to slope during the late Aptian-Albian time (Yıldız et al. 2017).

In the study area, the carbonates are affected by large-scale dolomitization and host the economic polymetallic mineralization as veins and lenses within or near its upper contact with the overlying formation (Akçay et al. 2011). Akçay et al. (2011) also reported that the Pb-Zn-Cu-Au-Ag mineralization co-exists with massive pyrite, sphalerite, galena, and chalcopyrite lenses. The Upper Cretaceous volcano-sedimentary sequence (Okay and Şahintürk, 1997) deposited in rift basins resembles the sequence of the magmatic arc but subduction polarity is still controversial (e.g., Dewey et al. 1973; Şengör and Yılmaz 1981; Bektaş et al. 1999; Eyuboglu et al. 2014). In the southern part of the Eastern Pontide, the sequence comprises of three different assemblages. The first assemblage, the lower part of the sequence, is represented by yellowish-colored, sandy limestones on the underlying platform carbonates. The second assemblage, which is nearly the middle part of the sequence grades upward to globotruncana- bearing red pelagic limestones. The third assemblage, which is the uppermost of the sequence, consists of dominantly of marl, claystone, siltstone, sandstone, micritic limestone alternations and locally with interbedded felsic tuff (Okay and Şahintürk 1997; Eyuboglu 2015). Lower Cenozoic rocks that unconformably overlie the Upper Cretaceous and older rocks are widely distributed in the northern part of the studied area. These units are mainly represented by basalt-andesite and associated pyroclastic rocks and Nummulite-bearing limestone (Arslan and Aliyazıcıoğlu 2001; Arslan and Aslan 2006; Eyuboglu et al. 2013). The youngest rocks of the study area are Eocene in age and consists of oval-shaped granitic intrusions (Eyuboglu et al. 2017).

Methods

Draft

Seventy-two samples were collected from Hazine Mağara 72 m thick-stratigraphic section of Upper Jurassic-Lower Cretaceous Berdiga Formation in Gümüşhane, (NE Turkey) (Fig. 1). The petrographic analysis was conducted on thin sections that were stained with alizarin-red S and potassium ferricyanide (Dickson 1966). Cathodoluminescence properties of selected samples were examined at the Istanbul Technical University with CITL (Cambridge Image Technology Ltd.) Cold Cathodoluminescence, Model 8200 Mk5-2 mounted on a Nikon Eclipse LV100-POL microscope integrated with an optical spectrometer (OS) and an energy-dispersive spectrometer (EDX). The system was operated at 10–20 kV and 450–500 mA conditions, and a vacuum was fixed at 100–1000 mbar. X-ray diffractometry (XRD) of selected samples was done with a Rigaku DMAX IIC x-ray diffractometer (Cu-Kα radiation ~35 kV, 15 mA). Scanning rate was 2º/min with 5–70º 2θ. Microthermometric measurements of fluid inclusions were carried out with Linkam THMSG-600 with the cooling/heating stage that was calibrated using Fluid Inc. synthetic standards. Temperatures of homogenization and last ice melting have standard errors of ±1 °C. Tm values were used to calculate salinity expressed as wt% NaCl equivalent (Bodnar, 1993): wt% NaCl = $1.78*T_m - 0.0442*(T_m)^2 + 0{,}000557*(T_m)^3$ (Bodnar 1993). SEM characteristics of selected samples were examined at the Science and Technology Application and Research Center (BİLTEM), Bozok University using FEI, Quanta FEG-450 scanning electron microscope integrated with an AMETEK-EDAX, Octane Plus Energy Dispersive Spectroscopy and Field Emission Gun. The system was operated at 10–20 kV and 450–500 mA conditions, and a vacuum were fixed at 100–1000 mbar.

Major, trace element and REE contents of selected samples were determined with the ICP-EAS (Inductively Coupled Plasma-Atomic Emission Spectrometer) method. Sample preparation (dissolving in acid and filtering) and measurements were conducted at ACME Analytical Laboratories Ltd. (Canada). Deduction limits of elements are 0.01% for Ca, Mg,

Draft

Na, and Fe and 5 ppm for Mn and Sr. The dolomite and belemnite samples (10–15 mg) were also analyzed for their oxygen and carbon isotope contents. The samples were reacted in vacuo with 100% pure phosphoric acid for at least 4 hours at 50°C for dolomite and 25°C for calcite. The extracted CO_2 gas was analyzed for isotopic ratios on a Thermo Finnigan Delta Plus Ion Ratio Mass Spectrometer (IRMS). Precision was 0.05‰ for both $\delta^{13}C$ and $\delta^{18}O$. The values of carbon and oxygen isotopes are reported in per mil (‰) relative to the VPDB (Vienna Pee Dee Belemnite) standard. These analyses were conducted at the Pacific Centre for Isotopic and Geochemical Research (PCIGR) laboratories of the Bristol Columbia University. $^{87}Sr/^{86}Sr$ isotope ratios of these samples were also measured at the same laboratory. The long-term measured value for SRM987 is 0.71026 ±0.000015 (1 SD). Concentrations were measured at Thermo Finnigan Element II, High-Resolution ICP-MS by using the method described by Pretorius et al. (2006). All measured REE concentrations of all replacive dolomites were normalized to Post-Archean Australian shale (PAAS) and the PAAS data from Taylor and McLennan, 1985. We use the following method: 1) Eu-anomaly = $Eu_N/(Sm_N+Gd_N)^{0.5}$ and 2) Ce anomaly= $Ce/Ce^*=3Ce_N/(2La_N+Nd_N)$ to test whether a real Eu and Ce anomaly exist (Bau and Dulski 1996; MacLeod and Irving 1996; Shields and Stille 2001; Lawrence et al. 2006).

Results

Petrography

A variety of diagenetic processes including calcite cementation, micritization, dolomitization, dolomite recrystallization, dissolution of dolomite, silicification and pyrite mineralization were observed in the Berdiga Formation carbonates. A paragenetic sequence is presented in Figure 2 based on petrographic observations and cross-cutting relationships. Diagenesis was initiated by early calcite cementation which occurs as very fine crystals

Draft

ranging between 10 μm and 50 μm in size. Calcite cementation is represented by two types: 1. fine crystalline isopachous rim cement, surrounding allochems which were strongly micritized, and 2. fine crystalline equant calcite cement, filling interparticle pores in grainstones (Fig.3a). All examined rocks are pervasively dolomitized. Pervasive dolomitization is represented by three different types of the replacive dolomite textures: (1) Microcrystalline planar-s dolomite (e.g. Sibley and Gregg, 1987) with crystal size ranging from 25 to 50 μm, replacing micritic matrix (called here microdolomite, Md; Fig. 3b). Micro-stylolites are observed crosscutting Md dolomites (Fig. 3b). (2) Fabric-preserving, fine to medium crystalline planar-s dolomite (Fpd, Fig. 3c). This type of dolomites generally replaced grainstone facies of the formation. (3) Fabric-destructive medium to coarse crystalline planar-s dolomite with crystal size ranging from 100 to 150 μm (Fdd, Fig. 3d). Crystals often have cloudy cores with clear rims under plane polarized light and sharp extinction under crossed polars. Low amplitude stylolites cut across Fdd dolomite (Fig. 3d). Md, Fdp and Fdd dolomites have an abundance of about 10–25%, 15-20%, 45-65% (volumetrically and respectively), but dolomite cement has a very minor abundance (< % 0.5). Dolomite cement (Cd) is rare and occurs in hairline fractures and vugs (Fig. 4a, c). Cd comprises of planar to non-planar crystals with a size in the range of 50–100 μm that exhibit a sharp extinction. Moreover, microcrystalline quartz also observed in dissolution vugs and occluding hairline fractures. Silicification is widespread in the upper part of the section. Evidence of dissolution of all type of dolomites observed along stylolites where the resulted porosity is filled by microcrystalline quartz and pyrite minerals (Fig. 4a-f and Fig. 5a-d). In addition, pyrite is the second common non-carbonate mineral observed within dissolution pore of replacive dolomite (Fig. 5a). The scattered euhedral pyrite crystals are very small (10-60 μm) euhedral and occlude vuggy pore spaces. In most samples, pyrite co-exists with microcrystalline quartz in the pore spaces.

Draft

205

206 **Fluid inclusions**

207 Fluid inclusion microthermometry data were obtained from Fdd Dolomite and dolomite
208 cement (Cd). Fluid inclusions are quite small (3- 6 μm in size) and have two phases (liquid
209 and vapor). Most of the fluid inclusions are represented by primary inclusions, but secondary
210 inclusions along the outer rim of crystal and micro-fractures are also observed. In these cases,
211 temperature data were recorded only from primary, two-phase liquid-vapor inclusions.
212 Homogenization temperatures of primary fluid inclusions in cloudy dolomite cores range
213 from 85 to 170 ^{o}C, and those distributed along growth zones (rims) are 160-230 ^{o}C for
214 replacive dolomite. However, dolomite cement shows a higher range of Th values from 200 to
215 240 ^{o}C. Last ice melting temperature of dolomites cannot be measured due to the small size of
216 the inclusions.

Draft

217

218 **Strontium isotopes**

219 Seventeen samples of belemnite shells and dolomites were analyzed for their strontium
220 isotopic composition. $^{87}Sr/^{86}Sr$ ratios of the belemnite shell range between 0.70739 and
221 0.70742 falling within the range of the Valanginian marine carbonate values (Veizer et al.
222 1999). Replacive dolomite $^{87}Sr/^{86}Sr$ ratios vary from 0.70753 to 0.70879 which are enriched
223 with respect to Valanginian marine carbonate values. In general, most dolomite types have
224 relatively higher Sr isotopes than the reported for Late Jurassic-Early Cretaceous seawater
225 values (Fig.7a) (Veizer et al. 1999).

226

227 **Stable carbon and oxygen isotopes**

228 Belemnite shells, collected from the Berdiga Formation, has $\delta^{18}O$ values ranging
229 between -2.51 and -1. 40 ‰ V-PDB, and $\delta^{13}C$ values spanning between 0.10 and 1.84 ‰ V-

PDB (Fig. 7b; Table 1). Both $\delta^{18}O$ and $\delta^{13}C$ values are in agreement with the range reported for postulated calcite precipitated from Late Jurassic- Early Cretaceous seawater (Veizer et al.1999; Veizer and Prokoph 2015). The approximated coeval marine dolomite spans from 0.34 to 2.44‰ using the equation of $\Delta^{18}O$ ($\delta^{18}O_{dolomite} - \delta^{18}O_{calcite\text{-}belemnite}$= 3.84‰ VPDB (e.g. Vahrenkamp and Swart 1994). Md dolomite possesses the highest $\delta^{18}O$ values (average -5.54 ‰, excluding one sample). Fpd dolomites show relatively lower $\delta^{18}O$ values (average -6.32‰). Fdd dolomite usually possesses the lowest $\delta^{18}O$ values (average -6.95‰) among all of the replacive dolomites. $\delta^{18}O$ values of Berdiga dolomites are much lower than those postulated values for dolomite precipitating from Late Jurassic–Early Cretaceous ocean water (Veizer et al. 1999). The $\delta^{13}C$ values of all replacive dolomites (0.69 to 3.13 ‰) are nearly similar to those of the belemnite sample (0.10 to 1.84‰) and matches up with values the estimated $\delta^{13}C$ (3.0 to 0‰VPDB) of calcite precipitated from the Late Jurassic-Early Cretaceous seawater (Qing and Veizer 1994; Veizer et al. 1999; Shields et al. 2003).

Major-trace and REE characteristics

Trace, major and rare earth elements are presented in Tables 1 and 2. All reported replacive dolomites show similar $CaCO_3$ contents ranging from 58 to 56 wt.%, $MgCO_3$ values between 42 and 44 wt.%. These dolomites are nonstoichiometric, calcium-rich and have but significantly high Fe (2727-21053 ppm; average 7451 ppm) and Mn (1548-9293; average 4946 ppm) contents. Moreover, a Fdd dolomite crystal was analyzed along the line from core to overgrowth rims (Fig. 6a-c). Generally, overgrowth rims show higher Fe and Mn values than the core (Fig. 6a-c). Further, most of them have relatively low Sr (56-243 ppm; average 88 ppm) and variable Na (74-222 ppm; average 162 ppm) contents. Overall REE abundances (∑REE) of replacive dolomites range from 6.4 to 41.2 ppm, which are higher than REE concentrations of belemnite samples. Dolomite samples have low Y/Ho ratios (23 to 43). The

Draft

REE patterns of all types are fairly similar and display various degrees of positive Eu anomaly (δEu), which ranges from 1.3 to 2.1 with average 1.6 and slightly flattened Ce anomaly (δCe) which ranges from 0.8 to 1.1 with average 0.9 (Fig.9a, b, c).

Discussion

Diagenesis

Petrographic and geochemical data indicate that Berdiga Formation has undergone a complex diagenetic history since its deposition. Different stages of diagenesis have been suggested to explain the shallow to deep burial diagenetic phases present in the Berdiga Formation (Fig. 2).

Early shallow burial stage

Upper Jurassic-Lower Cretaceous carbonates were deposited on an inner platform to deep shelf environments (e.g. Koch et al. 2008, Yıldız et al. 2017). Facies produced in such an environment is represented by non-laminated mudstone, foraminiferal grainstone/packstone, allochthonous bioclastic wackestone/mudstone microfacies (Yıldız et al. 2017). In the Berdiga Formation, diagenesis was initiated by micritization and early calcite cementation which occurs in grainstone microfacies (Fig. 3a). Micritization and calcite cementation are usually attributed to being linked to marine and very early shallow burial stage (Tucker and Wright 1990; Flügel 2004).

Early to medium burial stage

During the early shallow burial stage, the micrite of the mudstone facies was likely replaced by microdolomite (Fig. 3b). Petrographic evidence also supports this interpretation because microstylolites crosscut the microdolomite (Fig. 3b, d). With progressive burial,

Draft

grainstone/packstone facies are dolomitized by fabric preserving and fabric destructive dolomite; both are also crosscut by low amplitude stylolite. This crosscutting relationship of these dolomite types suggests that dolomitization likely formed during the early to medium burial stage before the onset of stylolitization. Stylolite generation ensues from increasing overburden stress and related increase of temperature during burial (e.g. Paganoni et al. 2016). Many researchers reported that the minimum depth of about 500 m is suggested for the formation of low amplitude stylolite generation (Dunnington 1967; Drivet and Mountjoy 1997; Duggan et al. 2001). If originally estimated thickness (at least 500-900m) of the Berdiga Formation is considered, dolomitization probably initiated in the buried lower part of the formation during the depositional time of the upper part of the sequence. At a time of deposition, the vertical movement of the syn-sedimentary extensional tectonic regime, which promoted deepening of the depositional environment during the late Aptian-Albian (e.g. Yıldız et al. 2017), probably resulted in fracturing-faulting of the carbonate platform. Fracture lines could provide suitable pathways for dolomitizing fluids and will facilitate pervasive dolomitization of the formation (Kırmacı et al. 2018). Fracture-filled dolomite cement is observed in Kuşakkaya area which is nearly 5 km west of the studied dolomites. This is also supported by huge dolomite bodies (i.e. a 500 m thick), which are located along the main fracture-fault lines and in parts of structural heights facing depression areas (Eren 1983; Kırmacı 1992).

Deep burial stage

Deep burial processes, which occurred during Eocene magmatic event (Eyuboglu et al. 2017), hot hydrothermal fluids circulated in the basin and resulted in recrystallization of MD, Fpd, and Fdd. Recrystallization of replacive dolomites have been suggested in previously published works (e.g. Martín-Martín 2015; Al-Aasm and Clarke 2004; Adam and Al-Aasm

Draft

2017). Recrystallization of dolomite may involve both textural as well as chemical modifications (Al-Aasm 2000). Gregg (2004) reported that unimodal size distribution of dolomite crystals and coarsening of crystal size can be indicative of the recrystallization. Similar petrographic characteristics are observed in the all replacive dolomite types (Fig.4.e and 5.b). The recrystallization of dolomite involved several geochemical changes including a negative shift in $\delta^{18}O$ isotopes (Kupecz et al. 1993). Assuming that the origin of dolomitizing fluids was remnant Late Jurassic-Early Cretaceous seawater, then the measured $\delta\ ^{18}O$ values are more depleted than calculated $\delta\ ^{18}O$ values for the replacive dolomites according to the dolomite-fluid fractionation equation (Fig. 7b) (0.6 to –2.9‰; Land 1983). Negative $\delta^{18}O$ values can be explained in terms of higher burial temperatures and/or variable isotopic fluid composition (Adam and Al-Aasm 2017; Al-Aasm and Crowe 2018). Based on the geochemical and petrographic evidence, it could be interpreted that replacive dolomite types recrystallized in a burial diagenetic environment and/or altered by hydrothermal fluids. Assuming a 30 ^{o}C/km geothermal gradient and a 20 ^{o}C surface temperature, a minimum of 2.5 km of sediments would have needed to support the maximum temperatures (95 ^{o}C), the sufficient depth of burial reached at the end of the Eocene time based on the thickness of the overlying formations (Kırmacı et al. 2018). This is also supported by the homogenization temperatures in the core of Fdd dolomite crystals (85-170) which necessitate such 2.2-4.5 km burial depth. Furthermore, a minimum homogenization temperature (160-230 ^{o}C) measured at the rim of Fdd dolomite requires that it is formed at a much deeper burial depth such as 4.7-7 km. However, the burial history of Berdiga Formation does not support such a depth, because maximum burial depth is estimated at 2.9 km (Kara-Gülbay et al. 2012). Therefore, the proposed temperatures could not be achieved by regional geothermal gradient alone, but instead are possibly caused by the Eocene magmatic generation which was widespread in the Eastern Pontide (Eyuboglu et al. 2017).

Draft

Therefore, the negative values of $\delta^{18}O$ of replacive dolomites are likely due to elevated temperatures during recrystallization related to hydrothermal effect induced by Eocene pluton. Moreover, all investigated dolomite samples have distinctly higher $^{87}Sr/^{86}Sr$ ratios than those reported for Late Jurassic-Early Cretaceous seawater (Fig. 7a). Hence, the radiogenic Sr isotopic composition might be related to the flux of hydrothermal fluids during the Eocene granitoid development. However, $^{87}Sr/^{86}Sr$ ratios of dolomites are higher than Eocene Pluton (0.70482 to 0.70548; Eyuboglu et al. 2017), which may have provided the acidic fluids for the hydrothermal alteration. Considering less radiogenic the $^{87}Sr/^{86}Sr$ values of the granitoid relatively to replacive dolomites (Karsli et al. 2007; Eyuboglu 2017), alteration fluids may have interacted with overlying siliciclastic rocks to pick up a radiogenic signal during its infiltrating process (e.g., Collins 1975; Banner 1995). McLennan at al. (1990) reported $^{87}Sr/^{86}Sr$ ratios varying from 0.7090 to 0.7340 for quartz sand in passive margin turbidites which are similar to the overlying formation in the study area. Therefore, diagenetic fluids became enriched in $^{87}Sr/^{86}Sr$ after circulating and interacting with siliciclastic rocks (Fig.7a). In addition, enrichment in Mn and Fe values of replacive dolomites support this scenario, because hydrothermal fluids could probably be interacted with underlying basaltic rocks of Şenköy Formation (these basaltic rocks are characterized by high thickness (roughly 50 m in the study area), and high FeO (4.89 to 10.73 wt.%) and MnO contents (0.08-0.15 wt.%; Arslan et al. 1999) or overlying basaltic rocks of Alibaba Formation (the basaltic rocks generally are represented by high thickness up to 500 m and their FeO and MnO contents vary from 2.69 to 12.13 wt.%, 0.09 to 0.20 wt.% respectively; Arslan et al. 1999) during the convectional circulation and altered fluid chemistry. Therefore, it could be predicted that they resulted in both epithermal veins polymetallic mineralization in the upper part of the formation and recrystallization of all dolomite types (Fig. 8a-c) (Kupecz et al. 1993; Akçay et. 2011). However, Warren (2000) proposed that later burial dolomites may have much higher

Draft

Fe and Mn levels owing to the reducing conditions than the early near-surface dolomite. Progressive burial in association with a reducing environment has favored Fe concentrations (Adam and Al-Aasm 2017). In the study area, not only microdolomite (Md) and fabric preserving dolomite (Fpd) dolomite formed at early burial environment, but also the formation of fabric destructive dolomite (Fdd) may occur at shallow to intermediate burial. However, Fe and Mn concentrations of all dolomite types are considerably higher than Başoba Yayla dolomites which are located in northern part of the Eastern Pontide and formed at shallow to intermediate burial depth (Kırmacı et al. 2018). Therefore, the extremely high Fe and Mn values are probably related to the epithermal vein polymetallic mineralization. Moreover, the overgrowth zone in Fdd dolomite crystal which was analyzed along the line from core to overgrowth rims (Fig. 6a-c) shows higher Fe and Mn values than the core. The elevated Mn and Fe concentrations support the hypothesis that hydrothermal fluids, which were associated with polymetallic mineralization could have been instrumental during recrystallization of earlier formed dolomite. Furthermore, mineralization is attributed to result in the magmatic generation produced in the Gümüşhane region during the Eocene (Akçay et al. 2011; Akaryali and Akbulut 2016). Akçay et al. (2011) which occurred within a wide range of temperatures (130–370 ^{o}C; average =240 ^{o}C). This has been confirmed by fluid inclusion analysis on quartz and barite which suggest epithermal conditions with low salinities (<8.5wt% NaCl eq.). Our fluid inclusion homogenization temperatures (up to 240 ^{o}C) measured in Cd dolomite and outer overgrowth rim of Fdd dolomites are in accordance with this previously published data.

The progressive enrichment in average ΣREE of diagenetic minerals and their similar REE patterns are generally controlled by diagenetic fluids with an increase in water/rock interaction ratio during the progressive burial (Haeri-Ardakani et al. 2013a, 2013b, 2013c; Qing and Mountjoy 1994a). However, concentrations of ΣREE of all replacive dolomite types

Draft

are higher than those of modern warm water brachiopods (Azmy et al. 2011; 0.05-0.73 ppm) and belemnite samples (Table 2). Therefore, all replacive dolomite types do not show REE seawater signatures and the elevated REE contents could be caused by recrystallizing fluids during the progressive burial. A possible source for higher ΣREE content in the Eastern Pontide is Eocene Granitoid whose ΣREE contents varies 126-138 ppm (Eyuboglu et al. 2017). Moreover, REE patterns of all dolomite types dolomites normalized to PAAS display distinct positive Eu anomaly, and slightly positive to negative Ce anomaly (Fig. 9a-c). Hollis et al. (2017) reported negative Ce and positive La anomalies, and slightly flattened HREE for fault-controlled dolomites, which reflect suboxic seawater signatures. Navarro-Ciurana et al. (2017) also reported similar REE characteristics of Riópar dolostones (Upper Jurassic to Lower Cretaceous) and these features are widely regarded as characteristic of marine carbonates formed from oxygen-rich shallow water fluids. Therefore, the negative Ce anomaly is widely regarded as a characteristic feature of seawater, but slightly flattened Ce anomaly could likely be a result of recrystallization with hydrothermal fluids due to the oxidative removal of Ce from seawater and incorporation into dolomites (e.g. Sholkovitz and Shen 1995; Azmy et al. 2013). Moreover, positive Eu anomaly in carbonates is a typical signature of the precipitation from or influence of hydrothermal fluids (Hecht et al. 1999; Frimmel 2009; Parsapoor et al. 2009). In addition, lower Y/Ho ratios (between 23 and 40) are also supporting hydrothermal alteration because Y and Ho can mobilize from host rocks into fluids during hydrothermal alteration (Fig. 9d) (e.g. Kučera et al. 2009). The lower Sr concentrations in replacive dolomites types compared to belemnite samples can be clues of the recrystallization (Fig. 8c) (e.g. Al-Aasm and Clarke 2004).

In summary, several petrographic and geochemical lines of evidence support recrystallization of dolomite due to the hydrothermal fluids associated with polymetallic mineralization including 1) depletion in $\delta^{18}O$ values with respect to Late Jurassic-Early

Draft

Cretaceous seawater; 2) radiogenic $^{87}Sr/^{86}Sr$ ratios; 3) extremely high Fe (2727-21053 ppm) and Mn (1548-27726 ppm) contents; 4) higher homogenization temperatures of fluid inclusions and elevated Mn /Fe values from core to rim; 5) slightly flattened Ce, positive Eu anomaly, and Y/Ho ratios; (6) presence of secondary pyrite and 7) unimodal size distribution and coarsening of dolomite crystal size.

Hydrothermal fluids which are associated with Pb–Zn mineralization might lead to not only recrystallization but also dissolution and precipitation of sulphides occurring mainly in the ore body and its immediate surroundings (Corbella et al. 2004; Appold and Garven 1999). Many researchers reported that circulation of acidic fluids derived from the granitic plutons and related mineral deposits could be the cause for the dissolution of carbonate minerals in deeper burial conditions (e.g. Martín-Martín et al. 2015). Silicification, which can be related to Eocene pluton, probably affected the studied section during deeper burial diagenetic processes as evidenced by silica replacement along the stylolites and vugs (Fig. 5. a-d). Furthermore, scattered, euhedral pyrite minerals (5-10 μm) are observed in vugs within all replacive dolomite types (Figs. 4b, d, f, and Fig. 5a). Moreover, similar CL patterns of the dolomite rim to Cd dolomites can indicate an alteration by fluids responsible for later cement dolomites (Fig. 4. a, c) (e.g. Chen et al. 2004; Guo et al. 2016).

Draft

Source of magnesium and dolomitization mechanism

Berdiga Formation has been pervasively dolomitized carbonates for a distance of meters to kilometers. Dolomite bodies are large volumes with irregular morphology. The dolomite bodies are located near or an along the main fault lines, which define the borders of early-Middle Jurassic rift basin, and in parts of structural heights facing depression areas (Eren 1983; Kırmacı 1992). Such a large-scale dolomitization replacing Upper Jurassic-Lower Cretaceous limestones has been reported in throughout the mid-latitude shallow water domain

of Tethys and several models which accounts for the source of dolomitizing fluids and mechanism have been suggested to explain the origin of pervasive dolomitization (e.g. Murgia et al. 2004, Iannace et al. 2011; Martín-Martín et al. 2015; Navarro-Ciurana 2016). The integrated petrographic, stable and Sr isotopes, geochemistry and fluid-inclusion microthermometry provided clues to the origin of pervasive dolomitization. During the Late Jurassic-Early Cretaceous, the study area was located within the platform environment on a passive continental margin of the northern branch of Neotethys (Görür 1988; Okay and Şahintürk 1997). In such a tectonic setting and warm equatorial-subequatorial paleoclimate conditions could enhance and facilitate evaporation (e.g., Friedrich et al. 2012). This scenario agrees in general with petrographic characteristics of Md, which is possibly formed at somewhat elevated temperatures (below 50^{o}C). Hence, it can be linked to penecontemporaneous to near-surface dolomitization (Gregg and Sibley 1984; Al-Aasm and Packard 2000; Warren 2000; Machel 2004). Therefore, sabkha environment could facilitate the dolomite precipitation/replacement for microdolomite (Md) from highly saturated brines by lowering the kinetic barriers at relatively elevated temperatures. However, the lack of primary evaporite minerals implies that hypersaline dolomitization model can be ruled out (e.g. Warren 2000). Moreover, the Na contents and the negative shift in the O isotopes of Md cannot be explained by this model. CL characteristics of Md (Fig. 4.c) points to the presence of Fe in the dolomitizing fluid (Pierson 1981; Machel and Burton 1991). Bacterial sulphate reduction model is generally considered to play a role in this kind of CL characteristics, but the lack of primary pyrite within intercrystalline pores of Md may indicate that this mechanism is not applicable for the formation Md (Vasconcelos and McKenzie 1997; Preto et al. 2015). Furthermore, petrographic characteristics of Fpd and Fdd show the absence of associated evaporites and pyrite minerals, and the negative shift in $\delta^{18}O$ values of these dolomites may imply that hypersaline dolomitization model can also be ruled out. If

Draft

dolomitization occurred in a mixing zone, then the $\delta^{13}C$ values of dolomite could not be explained. However, the $\delta^{13}C$ values of all dolomite types are highly similar to the postulated values for Late Jurassic-Early Cretaceous seawater (Veizer et al. 1999; Shields et al. 2003).

The other potential source for dolomitization to consider is dewatering of underlying facies which could have provided dolomitizing fluids for the overlying mudstone facies which have a high porosity and permeability during the early phase of the burial compaction (Mresah 1998). Taking into account that Berdiga Formation is composed of mostly mudstone and/or wackestone microfacies (Koch, et al. 2008), suggest that these fluids could have been the source for dolomitization. These kinds of dolomitizing fluids are also suggested by Kırmacı (2013) for the Upper Jurassic platform carbonates in the southern part of Turkey. However, Kırmacı et al. (2018) reported similar types of replacive dolomite as well as the other types in the Trabzon area (NE Turkey). Such a large-scale dolomitization generally necessitate high amounts of magnesium source in order to pervasively replace the host limestone (Machel 2004; Davies and Smith 2006). The large source of Mg in the underlying formation is not apparent in the study area and also the early to the medium stage of chemical compaction features, such as stylolites crosscuts all dolomite types. Therefore, burial compaction model cannot explain the origin of pervasive dolomites. On the other hand, the formation of replacive dolomites occurred in the early stage of burial history as evidenced by the presence of stylolites crosscutting Md and Fdd Dolomite (Kırmacı and Akdağ 2005; Adam and Al-Aasm 2017). Therefore, the petrographic evidence does not support the burial compaction model for all replacive dolomite types.

Mg sources for the pervasive dolomitization could have only been supplied by considerable volumes of seawater funneled through the main fault zone to the facies with high porosity and permeability (Fig. 10a). In similar conditions, Martín-Martín et al. (2013, 2015) and Gomez-Rivas et al. (2014) suggested that dolomitization of the Lower Cretaceous limestones is

Draft

attributed primarily to be controlled by the regional fault system in eastern Spain. Martín-Martín et al. (2015) also reported dolomites with δ ^{18}O values between -6.18 and -10.51‰, and δ ^{13}C values between 1.89 and 5.75‰, which are similar to the observed dolomites in this study (Table 1). Moreover, the majority of δ ^{13}C values of pervasive dolomite are in agreement with the range reported for Late Jurassic-Early Cretaceous seawater values suggesting that carbon was derived internally from the same seawater or host carbonates. Na concentrations of replacive dolomite types (74–220 ppm) are consistent with those deposited from normal seawater (about 110–160 ppm) (Veizer 1983; Qing and Mountjoy 1994b). The lower Na concentrations in a few samples are attributed recrystallization of dolomite by Na-depleted hydrothermal fluids (Kırmacı et al. 2018). Depletion in Sr concentrations (56–243 ppm) in replacive dolomite can be also related to recrystallization, because calcian dolomites which deposited from normal seawater, has nearly 250 ppm in Sr concentration (Fig. 7d) (e.g. Vahrenkamp and Swart 1990). However, high $^{87}Sr/^{86}Sr$ ratios (0.70753 to 0.70884), extremely high Fe (2727-21053 ppm), Mn (1548-27726 ppm) values, REE patterns of dolomites with distinct positive Eu anomaly and no significant Ce anomalies are not typical of dolomites formed for this setting, and original signatures could have been completely obliterated during recrystallization. All types of replacive dolomites have probably been recrystallized by hydrothermal fluids associated with polymetallic mineralization under high-temperature domain during the emplacement of Eocene magmatism (Fig. 10b).

Conclusions

Field, petrographic and geochemical data indicate that the Berdiga Formation has undergone a complex diagenetic history, from shallow to deep burial. Diagenesis was initiated by micritization and early calcite cementation in grainstone microfacies. With progressive burial, reactivation of extensional tectonics resulted in fracturing and faulting of the carbonate

Draft

platform and formation of small-scale horst/graben system from time to time. Fractures could have provided suitable pathways for dolomitizing fluids of seawater origin and facilitated pervasive dolomitization of the formation. Dolomitization is one of the most important processes which affected all sections. Three different types of the replacive dolomite textures are recognized: microdolomite (Md Dolomite), fabric preserving dolomite (Fpd Dolomite) and fabric destructive dolomite (Fdd Dolomite). Deeper burial processes, which occurred during magmatic event accompanied by hot hydrothermal fluids associated with emplacement of the polymetallic mineralization circulated in all dolomite and likely resulted in recrystallization. Recrystallization is the second important process affecting all dolomites. Moreover, hydrothermal fluids might lead not only recrystallization, but also dissolution, silicification, and pyrite mineralization.

Draft

Acknowledgments

The authors thank Karadeniz Technical University, Scientific Research Project Funding (KTU BAP, Project no: FBA-2015-5160) and Scientific and Technological Research Council of Turkey (TUBITAK-ÇAYDAG, Project no: 115Y005 and TUBITAK International Ph.D. Research Scholarship Program-2214-A-BIDEP) for their financial support. ISA acknowledge the support from NSERC. This work contains the part of geochemical findings of Ph.D. thesis undertaken by Merve Özyurt at the Institute of Sciences, Karadeniz Technical University, Turkey. Special thanks to Editor Dr. Ali Polat, Guest Editor Dr. Karem Azmy and reviewers for their effort to improve our paper. Thanks also due to Torun Yılmaz and Nurbanu Ergül for their help during the sampling period. Thanks also to Serhat Koçoğlu for his help with scanning electron microscope analysis. The appreciation is extended to Dr. Emin Çiftçi for his help for CL studies.

530

531 **References**

532

533 Adam, J., and Al-Aasm, I. S. 2017. Petrologic and geochemical attributes of calcite
534 cementation, dolomitization, and dolomite recrystallization: an example from the
535 Mississippian Pekisko Formation, west-central Alberta. Bulletin of Canadian Petroleum
536 Geology, 65: 235-261.

537 Akaryali, E., & Akbulut, K. 2016. Constraints of C–O–S isotope compositions and the origin
538 of the Ünlüpınar volcanic-hosted epithermal Pb–Zn±Au deposit, Gümüşhane, NE
539 Turkey. Journal of Asian Earth Sciences, 117: 119-134.

540 Akçay, M., Gündüz, Ö., Yaşar, R. and Gümrük, O. 2011. Geochemical and Genetic Features
541 of Hazinemağara and Kirkpavli (Gümüşhane) Polymetallic Pb-Zn-Cu-Au-Ag Deposits.
542 64th Geological Congress of Turkey, Ankara, Turkey, TJK Bilidiri Özleri Kitabı,

543 Al-Aasm, I. 2003. Origin and characterization of hydrothermal dolomite in the Western
544 Canada Sedimentary Basin. Journal of Geochemical Exploration, 78: 9-15.

545 Al-Aasm, I. S., and Clarke, J. D. 2004. The effect of hydrothermal fluid flow on early
546 diagenetic dolomitization: an example from the Devonian Slave Point Formation,
547 northwest Alberta, Canada. AAPG Special Volumes, doi:10.1306/1025696H13122, 297-
548 316

549 Al-Aasm, I. S., and Crowe, R. 2018. Fluid compartmentalization and dolomitization in the
550 Cambrian and Ordovician successions of the Huron Domain, Michigan Basin. Marine
551 and Petroleum Geology, 92: 160-178.

552 Al-Aasm, I. S., and Packard, J. J. 2000. Stabilization of early-formed dolomite: a tale of
553 divergence from two Mississippian dolomites. Sedimentary Geology, 131: 97-108.

Draft

554 Al-Aasm, I., Lonnee, J., and Clarke, J. 2000. Multiple fluid flow events and the formation of
555 saddle dolomite: examples from Middle Devonian carbonates of the Western Canada
556 Sedimentary Basin. Journal of Geochemical Exploration, 69: 11-15.
557 Al-Aasm, I. S., and J. J. Packard. 2000. Stabilization of early-formed dolomite: a tale of
558 divergence from two Mississippian dolomites. Sedimentary Geology 131: 97-108.
559 Appold, M. S., and Garven, G. 1999. The hydrology of ore formation in the Southeast
560 Missouri District; numerical models of topography-driven fluid flow during the Ouachita
561 Orogeny. Economic Geology, 94: 913-935.
562 Arslan, M., Tüysüz, N., Korkmaz, S., and Kurt, H. 1997. Geochemistry and petrogenesis of
563 the eastern Pontide volcanic rocks, Northeast Turkey. Chemie der Erde, 57: 157-188.
564 Arslan, M., and Aliyazicioglu, I. 2001. Geochemical and petrological characteristics of the
565 Kale (Gümüshane) volcanic rocks: implications for the Eocene evolution of eastern
566 Pontide arc volcanism, northeast Turkey. International Geology Review, 43: 595-610.
567 Arslan, M., and Aslan, Z. 2006. Mineralogy, petrography and whole-rock geochemistry of the
568 Tertiary granitic intrusions in the Eastern Pontides, Turkey. Journal of Asian Earth
569 Sciences, 27: 177-193.
570 Azmy, K., Brand, U., Sylvester, P., Gleeson, S. A., Logan, A., & Bitner, M. A. 2011.
571 Biogenic and abiogenic low-Mg calcite (bLMC and aLMC): Evaluation of seawater-REE
572 composition, water masses and carbonate diagenesis. Chemical Geology, 280: 180-190.
573 Azmy, K., Lavoie, D., Wang, Z., Brand, U., Al-Aasm, I., Jackson, S., and Girard, I. 2013.
574 Magnesium-isotope and REE compositions of Lower Ordovician carbonates from eastern
575 Laurentia: implications for the origin of dolomites and limestones. Chemical
576 Geology, 356: 64-75.

Draft

577 Azomani, E., Azmy, K., Blamey, N., Brand, U., and Al-Aasm, I. 2013. Origin of Lower
578 Ordovician dolomites in eastern Laurentia: controls on porosity and implications from
579 geochemistry. Marine and Petroleum Geology, 40: 99-114.
580 Banner, J. L. 1995. Application of the trace element and isotope geochemistry of strontium to
581 studies of carbonate diagenesis. Sedimentology, 42: 805-824.
582 Banner, J. L., Hanson, G. N., and Meyers, W. J. 1988. Rare earth element and Nd isotopic
583 variations in regionally extensive dolomites from the Burlington-Keokuk Formation
584 (Mississippian): Implications for REE mobility during carbonate diagenesis. Journal of
585 Sedimentary Petrology, 58: 415-432
586 Bau, M., & Alexander, B. 2006. Preservation of primary REE patterns without Ce anomaly
587 during dolomitization of Mid-Paleoproterozoic limestone and the potential re-
588 establishment of marine anoxia immediately after the "Great Oxidation Event". South
589 African Journal of Geology, 109: 81-86.
590 Bau, M., & Dulski, P. 1996. Distribution of yttrium and rare-earth elements in the Penge and
591 Kuruman iron-formations, Transvaal Supergroup, South Africa. Precambrian
592 Research, 79: 37-55.
593 Bektaş, O., Şen, C., Atici, Y., and Köprübaşi, N. 1999. Migration of the Upper Cretaceous
594 subduction-related volcanism towards the back-arc basin of the eastern Pontide magmatic
595 arc (NE Turkey). Geological Journal, 34: 95-106.
596 Bodnar, R. J. 1993. Revised equation and table for determining the freezing point depression
597 of H2O-NaCl solutions. Geochimica et Cosmochimica Acta, 57: 683-684.
598 Budd, D. A. 1997. Cenozoic dolomites of carbonate islands: their attributes and origin. Earth-
599 Science Reviews, 42: 1-47.

Draft

600 Chen, D., Qing, H., and Yang, C. 2004. Multistage hydrothermal dolomites in the Middle
601 Devonian (Givetian) carbonates from the Guilin area, South China. Sedimentology, 51:
602 1029-1051.
603 Collins, A. 1975. Geochemistry of oilfield waters, Developments in Petroleum Science1:
604 Elsevier. New York, 485 p.
605 Congwei, J. I., Hairuo, Q. I. N. G., Daizhao, C. H. E. N., Ping, L. U. O., Zhijun, J. I. N., and
606 Longyi, S. H. A. O. 2013. Characteristics and dolomitization of Upper Cambrian to
607 Lower Ordovician dolomite from outcrop in keping uplift, Western Tarim Basin,
608 Northwest China. Acta Geologica Sinica (English Edition), 87: 1005-1018.
609 Corbella, M., Ayora, C., Cardellach, E. 2004. Hydrothermal mixing, carbonate dissolution
610 and sulfide precipitation in Mississippi Valley-type deposits. Mineralium Deposita, 39:
611 344-357.
612 Davies, G. R., and Smith Jr, L. B. 2006. Structurally controlled hydrothermal dolomite
613 reservoir facies: An overview. AAPG Bulletin, 90: 1641-1690.
614 Dewey, J. F., PITMAN III, W. C., Ryan, W. B., & Bonnin, J. 1973. Plate tectonics and the
615 evolution of the Alpine system. Geological Society of America Bulletin, 84: 3137-3180.
616 Dickson, J. A. D. 1966. Carbonate identification and genesis as revealed by staining. Journal
617 of Sedimentary Research, 36: 491-505
618 Drivet, E., and Mountjoy, E. W. 1997. Dolomitization of the Leduc Formation (Upper
619 Devonian), southern Rimbey-Meadowbrook reef trend, Alberta. Journal of Sedimentary
620 Research, 67: 411-423.
621 Duggan, J. P., Mountjoy, E. W., and Stasiuk, L. D. 2001. Fault-controlled dolomitization at
622 Swan Hills Simonette oil field (Devonian), deep basin west-central Alberta,
623 Canada. Sedimentology, 48: 301-323.

Draft

624 Dunnington, H. V. 1967. Aspects of diagenesis and shape change in stylolitic limestone
625 reservoirs. In 7th World Petroleum Congress. World Petroleum Congress.
626 Eren, M. 1983. Gümüşhane-Kale arasının jeolojisi ve mikrofasiyes incelemesi, M. Sci.
627 Thesis, Karadeniz Üniversitesi, Trabzon, 197 p., (in Turkish with English abstract).
628 Eyuboglu, Y. 2015. Petrogenesis and U–Pb zircon chronology of felsic tuffs interbedded with
629 turbidites (Eastern Pontides Orogenic Belt, NE Turkey): Implications for Mesozoic
630 geodynamic evolution of the eastern Mediterranean region and accumulation rates of
631 turbidite sequences. Lithos, 212: 74-92.
632 Eyuboglu, Y., Dudas, F. O., Thorkelson, D., Zhu, D. C., Liu, Z., Chatterjee, N., Yi K., and
633 Santosh, M. 2017. Eocene granitoids of northern Turkey: Polybaric magmatism in an
634 evolving arc–slab window system. Gondwana Research, 50: 311-345.
635 Eyuboglu, Y., Santosh, M., Dudas, F. O., Akaryalı, E., Chung, S. L., Akdağ, K., and Bektaş,
636 O. 2013. The nature of transition from adakitic to non-adakitic magmatism in a slab
637 window setting: a synthesis from the eastern Pontides, NE Turkey. Geoscience
638 Frontiers, 4: 353-375.
639 Eyuboglu, Y., Santosh, M., Yi, K., Tuysuz, N., Korkmaz, S., Akaryali, E., and Bektas, O.
640 2014. The Eastern Black Sea-type volcanogenic massive sulfide deposits: Geochemistry,
641 zircon U–Pb geochronology and an overview of the geodynamics of ore genesis. Ore
642 Geology Reviews, 59: 29-54.
643 Flügel, E. 2004. Microfacies analysis of carbonate rocks. Analysis, interpretation, and
644 application. Springer, Berlin.
645 Friedrich, O., Norris, R. D., and Erbacher, J. 2012. Evolution of middle to Late Cretaceous
646 oceans—a 55 my record of Earth's temperature and carbon cycle. Geology, 40: 107-110.
647 Frimmel, H. E. 2009. Trace element distribution in Neoproterozoic carbonates as
648 paleoenvironmental indicator. Chemical Geology, 258: 338-353.

Draft

649 Garven, G. 1985. The role of regional fluid flow in the genesis of the Pine Point deposit,
650 western Canada sedimentary basin. Economic Geology, 80: 307-324.
651 Gomez-Rivas, E., Corbella, M., Martín-Martín, J. D., Stafford, S. L., Teixell, A., Bons, P. D.,
652 … and Cardellach, E. 2014. Reactivity of dolomitizing fluids and Mg source evaluation
653 of fault-controlled dolomitization at the Benicassim outcrop analogue (Maestrat Basin, E
654 Spain). Marine and Petroleum Geology, 55: 26-42.
655 Goodell, H. G., & Garman, R. K. 1969. Carbonate geochemistry of Superior deep test well,
656 Andros Island, Bahamas. AAPG Bulletin, 53: 513-536.
657 Görür, N. 1988. Timing of opening of the Black Sea basin. Tectonophysics, 147: 247-262.
658 Gregg, J. M. 2004. Basin fluid flow, base-metal sulphide mineralization and the development
659 of dolomite petroleum reservoirs. Geological Society, London, Special Publications, 235:
660 157-175.
661 Gregg, J. M., and Sibley, D. F. 1984. Epigenetic dolomitization and the origin of xenotopic
662 dolomite texture. Journal of Sedimentary Research, 54: 908-931.
663 Gregg, J. M., Bish, D. L., Kaczmarek, S. E., and Machel, H. G. 2015. Mineralogy, nucleation
664 and growth of dolomite in the laboratory and sedimentary environment: a
665 review. Sedimentology, 62: 1749-1769.
666 Gregg, J. M., Bish, D. L., Kaczmarek, S. E., and Machel, H. G. 2015. Mineralogy, nucleation,
667 and growth of dolomite in the laboratory and sedimentary environment: a
668 review. Sedimentology, 62: 1749-1769.
669 Guo, C., Chen, D., Qing, H., Dong, S., Li, G., Wang, D., ... and Liu, C. 2016. Multiple
670 dolomitization and later hydrothermal alteration on the Upper Cambrian-Lower
671 Ordovician carbonates in the northern Tarim Basin, China. Marine and Petroleum
672 Geology, 72: 295-316.

Draft

673 Güven, İ. H. 1998. 1/100000 ölçekli açınsama nitelikli Türkiye Jeoloji Haritaları, No: 59,
674 MTA, Ankara.
675 Haeri-Ardakani, O., Al-Aasm, I., and Coniglio, M. 2013 a. Petrologic and geochemical
676 attributes of fracture-related dolomitization in Ordovician carbonates and their spatial
677 distribution in southwestern Ontario, Canada. Marine and Petroleum Geology, 43: 409-
678 422.
679 Haeri-Ardakani, O., Al-Aasm, I., and Coniglio, M. 2013 b. Fracture mineralization and fluid
680 flow evolution: an example from Ordovician–Devonian carbonates, southwestern
681 Ontario, Canada. Geofluids, 13: 1-20.
682 Haeri-Ardakani, O., Al-Aasm, I., Coniglio, M., and Samson, I. 2013 c. Diagenetic evolution
683 and associated mineralization in Middle Devonian carbonates, southwestern Ontario,
684 Canada. Bulletin of Canadian Petroleum Geology, 61: 41-58.
685 Hecht, L., Freiberger, R., Gilg, H. A., Grundmann, G., and Kostitsyn, Y. A. 1999. Rare earth
686 element and isotope (C, O, Sr) characteristics of hydrothermal carbonates: genetic
687 implications for dolomite-hosted talc mineralization at Göpfersgrün (Fichtelgebirge,
688 Germany). Chemical Geology, 155: 115-130.
689 Hollis, C., Bastesen, E., Boyce, A., Corlett, H., Gawthorpe, R., Hirani, J., ... and Whitaker, F.
690 2017. Fault-controlled dolomitization in a rift basin. Geology, 45: 219-222.
691 Iannace, A., Capuano, M., and Galluccio, L. 2011. “Dolomites and dolomites” in Mesozoic
692 platform carbonates of the Southern Apennines: Geometric distribution, petrography, and
693 geochemistry. Palaeogeography, Palaeoclimatology, Palaeoecology, 310: 324-339.
694 Jiang, W. J., Hou, M. C., Xing, F. C., Xu, S. L., and Li, L. B. 2016. Characteristics and
695 indications of rare earth elements in dolomite of the Cambrian Loushanguan Group, SE
696 Sichuan Basin. Oil & Gas Geology, 37: 473-482.

Draft

Kara-Gülbay, R., Kırmacı, M. Z., and Korkmaz, S. 2012. Organic geochemistry and depositional environment of the Aptian bituminous limestone in the Kale Gümüşhane area (NE-Turkey): An example of lacustrine deposits on the platform carbonate sequence. Organic Geochemistry, 49: 6-17.

Karsli, O., Chen, B., Aydin, F., and Şen, C. 2007. Geochemical and Sr–Nd–Pb isotopic compositions of the Eocene Dölek and Sariçiçek Plutons, Eastern Turkey: implications for magma interaction in the genesis of high-K calc-alkaline granitoids in a post-collision extensional setting. Lithos, 98: 67-96.

Ketin, İ. 1966. Anadolu'nun tektonik birlikleri. Maden Tetkik ve Arama Dergisi, 66: 20-34.

Kırmacı, M. Z. 2013. Origin of dolomite in the Upper Jurassic platform carbonates, Bolkar Mountains, Central Taurides, Turkey: Petrographic and geochemical evidence. Chemie der Erde-Geochemistry, 73: 383-398.

Kırmacı, M. Z., and Akdağ, K. 2005. Origin of dolomite in the Late Cretaceous-Paleocene limestone turbidites, eastern Pontides, Turkey. Sedimentary Geology, 181: 39-57.

Kırmacı, M. Z., Yıldız, M., Kandemir, R., and Eroğlu-Gümrük, T. 2018. Multistage dolomitization in Upper Jurassic–Lower Cretaceous platform carbonates (Berdiga Formation), Başoba Yayla (Trabzon), NE Turkey: Implications of the generation of magmatic arc on dolomitization. Marine and Petroleum Geology, 89: 515-529.

Kırmacı, M.Z. 1992. Sedimentological investigation of the Upper Jurassic-Lower Cretaceous Berdiga Limestone in the Alucra-Gümüşhane-Bayburt regions Eastern Pontides, NE, Turkey. Ph.D. Thesis, Karadeniz Technical University, Trabzon (unpublished) (in Turkish with English abstract).

Kirmaci, M. Z., Koch, R., and Bucur, J. I. 1996. An Early Cretaceous section in the Kircaova Area (Berdiga Limestone, NE-Turkey) and its correlation with platform carbonates in W-Slovenia. Facies, 34: 1-21.

Draft

722 Koch, R., Bucur, I. I., Kirmaci, M. Z., Eren, M., and Tasli, K. 2008. Upper Jurassic and
723 Lower Cretaceous carbonate rocks of the Berdiga Limestone–Sedimentation on an
724 onbound platform with volcanic and episodic siliciclastic influx. Biostratigraphy, facies,
725 and diagenesis (Kircaova, Kale-Gümüşhane area; NE-Turkey). Neues Jahrbuch für
726 Geologie und Paläontologie-Abhandlungen, 247: 23-61.
727 Kučera, J., Cempírek, J., Dolníček, Z., Muchez, P., and Prochaska, W. 2009. Rare earth
728 elements and yttrium geochemistry of dolomite from post-Variscan vein-type
729 mineralization of the Nízký Jeseník and Upper Silesian Basins, Czech Republic. Journal
730 of Geochemical Exploration, 103: 69-79.
731 Kupecz, J. A., Montanez, I. P., & Gao, G. (1993). Recrystallization of dolomite with time.
732 (In: Carbonate microfabrics). Springer, New York, NY. 187-193
733 Land, L.S. 1983. The Application of stable isotopes to studies of the origin of dolomite and
734 problems of diagenesis of clastic sediments. In: Arthur, M.A., et al., Eds., Stable Isotope
735 in Sedimentary Geology, SEPM Short Course 10: 4.1-4.22.
736 Lawrence, M. G., Greig, A., Collerson, K. D., and Kamber, B. S. 2006. Rare earth element
737 and yttrium variability in South East Queensland waterways. Aquatic Geochemistry, 12:
738 39-72.
739 Leach, L.F., and Sangster, D.F. 1993. Mississippi valley-type lead-zinc deposits. In: Kirkham,
740 R.V., Sinclair, W.D., Thorpe, R.I., Duke, J.M. (Eds.), Mineral Deposits Modelling,
741 Geological Association of Canada Special Paper, 289-314.
742 Machel, H. G. 2004. Concepts and models of dolomitization: a critical reappraisal. Geological
743 Society, London, Special Publications, 235: 7-63.
744 Machel, H.G., Burton, E.A. 1991. Factors governing cathodoluminscence in calcite and
745 dolomite, and their implications for studies of carbonate diagenesis. - In: Barker, C.E. and

Draft

Kopp, O.C. (eds.): Luminescence microscopy and spectroscopy: qualitative and quantitative applications. Soc. Econ. Paleont. Min. Short Course, 25: 37-57.

MacLeod, K. G., & Irving, A. J. 1996. Correlation of cerium anomalies with indicators of paleoenvironment. Journal of Sedimentary Research, 66: *948-955*.

Martin, J. D. M., Travé, A., Gomez-Rivas, E., Salas, R., Sizun, J. P., Vergés, J., and Alfonso, P. 2015. Fault-controlled and stratabound dolostones in the late Aptian-earliest Albian Benassal Formation (Maestrat Basin, E Spain): Petrology and geochemistry constrains. Marine and Petroleum Geology, 65: 83-102.

Martín-Martín, J. D., Gomez-Rivas, E., Bover-Arnal, T., Travé, A., Salas, R., Moreno-Bedmar, J. A., and Stafford, S. L. 2013. The Upper Aptian to Lower Albian syn-rift carbonate succession of the southern Maestrat Basin (Spain): Facies architecture and fault-controlled stratabound dolostones. Cretaceous Research, 41: 217-236.

McLennan, S. M., Taylor, S. R., McCulloch, M. T., and Maynard, J. B. 1990. Geochemical and Nd-Sr isotopic composition of deep-sea turbidites: crustal evolution and plate tectonic associations. Geochimica et Cosmochimica Acta, 54: 2015-2050.

Morrow, D. W. 2014. Zebra and boxwork fabrics in hydrothermal dolomites of northern Canada: Indicators for dilational fracturing, dissolution or in situ replacement? Sedimentology, 61: 915-951.

Morrow, D. W., and Potter, J. 1998. Internal stratigraphy, petrography and porosity development of the Manetoe Dolomite in the region of the Pointed Mountain and Kotaneelee gas fields. Oil and gas pools of the Western Canada sedimentary basin: Canadian Society of Petroleum Geology Special Publication, 51: 137-161.

Mresah, M. H. 1998. The massive dolomitization of platformal and basinal sequences: proposed models from the Paleocene, Northeast Sirte Basin, Libya. Sedimentary Geology, 116: 199-226.

Draft

771 Muchez, P., Heijlen, W., Banks, D., Blundell, D., Boni, M., and Grandia, F. 2005.
772 Extensional tectonics and the timing and formation of basin-hosted deposits in
773 Europe. Ore Geology Reviews, 27: 241-267.
774 Muchez, P., Sintubin, M., and Swennen, R. 2000. Origin and migration pattern of palaeofluids
775 during orogeny: discussion on the Variscides of Belgium and northern France. Journal of
776 Geochemical Exploration, 69: 47-51.
777 Murgia, M. V., Ronchi, P., and Ceriani, A. 2004. Dolomitization processes and their
778 relationships with the evolution of an orogenic belt (Central Apennines and peri-adriatic
779 foreland, Italy). In: Deformation, Fluid Flow, and Reservoir Appraisal in Foreland Fold
780 and Thrust Belts, AAPG Hedberg Series, No. 1: 277-296.
781 Murray, R. W., Brink, M. R. B., Brumsack, H. J., Gerlach, D. C., and Russ III, G. P. 1991.
782 Rare earth elements in Japan Sea sediments and diagenetic behavior of Ce/Ce∗: results
783 from ODP Leg 127. Geochimica et Cosmochimica Acta, 55: 2453-2466.
784 Navarro-Ciurana, D., Cardellach, E., Galindo, C., Fuenlabrada, J. M., Griera, A., Gómez-
785 Gras, D., ... and Corbella, M. 2017. REE and Sm-Nd clues of high-temperature fluid-rock
786 interaction in the Riópar dolomitization (SE Spain). Procedia Earth and Planetary
787 Science, 17: 448-451.
788 Navarro-Ciurana, D., Corbella, M., Cardellach, E., Vindel, E., Gómez-Gras, D., and Griera,
789 A. 2016. Petrography and geochemistry of fault-controlled hydrothermal dolomites in the
790 Riópar area (Prebetic Zone, SE Spain). Marine and Petroleum Geology, 71: 310-328.
791 Nothdurft, L. D., Webb, G. E., and Kamber, B. S. 2004. Rare earth element geochemistry of
792 Late Devonian reefal carbonates, Canning Basin, Western Australia: confirmation of a
793 seawater REE proxy in ancient limestones. Geochimica et Cosmochimica Acta, 68: 263-
794 283.

Draft

795 Okay, A.I. and Şahintürk, Ö. 1997. Geology of the Eastern Pontides. In: Robinson, A. (Ed.),
796 Regional and Petroleum Geology of the Black Sea and Surrounding Regions. AAPG
797 Memoir, 68: 291-311.
798 Okay, A. I., and Tüysüz, O. 1999. Tethyan sutures of northern Turkey. Geological Society,
799 London, Special Publications, 156: 475-515.
800 Paganoni, M., Al Harthi, A., Morad, D., Morad, S., Ceriani, A., Mansurbeg, H., ... and Sirat,
801 M. 2016. Impact of stylolitization on diagenesis of a Lower Cretaceous carbonate
802 reservoir from a giant oilfield, Abu Dhabi, United Arab Emirates. Sedimentary
803 Geology, 335: 70-92.
804 Parsapoor, A., Khalili, M., and Mackizadeh, M. A. 2009. The behaviour of trace and rare
805 earth elements (REE) during hydrothermal alteration in the Rangan area (Central
806 Iran). Journal of Asian Earth Sciences, 34: 123-134.
807 Pelin, S. 1977. Geology and Petroleum Possibilities of Southeastern Alucra (Giresun) Region.
808 Karadeniz Technical University, Trabzon, Publication 87 (in Turkish with English
809 abstract).
810 Pierson, B. J. 1981. The control of cathodoluminescence in dolomite by iron and
811 manganese. Sedimentology, 28: 601-610.
812 Preto, N., Breda, A., Dal Corso, J., Spötl, C., Zorzi, F., and Frisia, S. 2015. Primary dolomite
813 in the Late Triassic Travenanzes Formation, Dolomites, Northern Italy: facies control and
814 possible bacterial influence. Sedimentology, 62: 697-716.
815 Qing, H., and Mountjoy, E. 1994a. Rare-earth element geochemistry of dolomites in the
816 Presqu'ile barrier and implications for water/rock ratio during
817 dolomitization. Sedimentology, 41: 787-804.

Draft

Qing, H., and Mountjoy, E. W. 1994b. Formation of coarsely crystalline, hydrothermal dolomite reservoirs in the Presqu'ile barrier, Western Canada sedimentary basin. AAPG Bulletin, 78: 55-77.

Qing, H., and Veizer, J. 1994. Oxygen and carbon isotopic composition of Ordovician brachiopods: Implications for coeval seawater. Geochimica et Cosmochimica Acta, 58: 4429-4442.

Shields, G. A., Carden, G. A., Veizer, J., Meidla, T., Rong, J. Y., and Li, R. Y. 2003. Sr, C, and O isotope geochemistry of Ordovician brachiopods: A major isotopic event around the Middle-Late Ordovician transition. Geochimica et Cosmochimica Acta, 67: 2005-2025.

Shields, G., & Stille, P. 2001. Diagenetic constraints on the use of cerium anomalies as palaeoseawater redox proxies: an isotopic and REE study of Cambrian phosphorites. Chemical Geology, 175: 29-48.

Sholkovitz, E., and Shen, G. T. 1995. The incorporation of rare earth elements in modern coral. Geochimica et Cosmochimica Acta, 59: 2749-2756.

Sibley, D. F., and Gregg, J. M. 1987. Classification of dolomite rock textures. Journal of Sedimentary Research, 57: 967-975

Şengör, C. A. M., & Yilmaz, Y. (1981). Tethyan evolution of Turkey: a plate tectonic approach. Tectonophysics, 75: 181-241.

Taslı, K., (1991). Stratigraphy, paleogeography, and micropaleontology of Upper Jurassic–Lower Cretaceous carbonate sequence in the Gümüşhane and Bayburt areas (NE Turkey). Ph.D. Thesis, Karadeniz Technical University, Trabzon (unpublished) (in Turkish with English abstract).

Draft

841 Taslı, K., Özer, E., and Yılmaz, C. 2000. Biostratigraphic and Environmental Analysis of the
842 Upper Jurassic-Lower Cretaceous Carbonate Sequence in the Başoba Yayla Area
843 (Trabzon, NE Turkey). Turkish Journal of Earth Sciences, 8: 125-135.
844 Taylor, S. R. and McLennan, S. M. 1985. The Continental Crust: Its Composition and
845 Evolution, Blackwell Scientific Publications, Oxford.
846 Tucker, M. E., and Wright, V. P. 2009. Carbonate sedimentology. Blackwell Scientific
847 Publications, Oxford.
848 Vahrenkamp, V. C., and Swart, P. K. 1990. New distribution coefficient for the incorporation
849 of strontium into dolomite and its implications for the formation of ancient
850 dolomites. Geology, 18: 387-391.
851 Vahrenkamp, V. C., and Swart, P. K. 1994. Late Cenozoic dolomites of the Bahamas:
852 metastable analogues for the genesis of ancient platform dolomites. In B. Purser (Ed.),
853 Dolomites: a volume in honour of Dolomieu. Blackwell Scientific; IAS Special
854 Publication, 21: 133-153
855 Vasconcelos, C., and McKenzie, J. A. 1997. Microbial mediation of modern dolomite
856 precipitation and diagenesis under anoxic conditions (Lagoa Vermelha, Rio de Janeiro,
857 Brazil). Journal of sedimentary Research, 67: 378-391.
858 Veizer, J. 1983. Trace elements and isotopes in sedimentary carbonates. Reviews in
859 Mineralogy and Geochemistry, 11: 265-299.
860 Veizer, J., and Prokoph, A. 2015. Temperatures and oxygen isotopic composition of
861 Phanerozoic oceans. Earth-Science Reviews, 146: 92-104.
862 Veizer, J., Ala, D., Azmy, K., Bruckschen, P., Buhl, D., Bruhn, F., and Jasper, T. 1999.
863 $^{87}Sr/^{86}Sr$, $\delta^{13}C$ and $\delta^{18}O$ evolution of Phanerozoic seawater. Chemical Geology, 161: 59-
864 88.

Draft

Warren, J. 2000. Dolomite: occurrence, evolution and economically important associations. Earth-Science Reviews, 52: 1-81.

Webb, G. E., and Kamber, B. S. 2011. Trace element Geochemistry as a tool for interpreting microbialites. In *Earliest* Life on Earth: Habitats, Environments, and Methods of Detection Springer, Dordrecht, 127-170.

Webb, G. E., Nothdurft, L. D., Kamber, B. S., Kloprogge, J. T., and Zhao, J. X. 2009. Rare earth element geochemistry of scleractinian coral skeleton during meteoric diagenesis: a sequence through neomorphism of aragonite to calcite. Sedimentology, 56: 1433-1463.

Wendte, J., Dravis, J. J., Stasiuk, L. D., Qing, H., Moore, S. L., and Ward, G. 1998. High-temperature saline (thermoflux) dolomitization of Devonian Swan Hills platform and bank carbonates, Wild River area, west-central Alberta. Bulletin of Canadian Petroleum Geology, 46: 210-265.

Yang, X., Mei, Q., Wang, X., Dong, Z., Li, Y., and Huo, F. 2018. Indication of rare earth element characteristics to dolomite Petrogenesis—A case study of the fifth member of Ordovician Majiagou Formation in the Ordos Basin, central China. Marine and Petroleum Geology. 92:1028-1040

Yıldız, M., Kırmacı, M. Z., Kandemir R. and Taslı K. 2017. "Benthic Foraminiferal Assemblages and Facies Analysis of the Late Jurrasic-Early Cretaceous Platform Carbonate Succession in the Mescitli-İkisu Area (Gümüşhane, NE Turkey)", Digital Proceeding of ICOCEE, pp.3550-3557.

Draft

Figure Captions

Figure 1. Location (A, B) and geological map of the study area (C) (modified after Güven, 1998).

Figure 2. Paragenetic sequence of the studied formation showing early to late diagenetic processes.

Figure 3. Photomicrographs of studied sections: a) grainstone facies. Mic: micritized allochem, Cc: Calcite cement; b) Microdolomite (Mc) which is microcrystalline planar-s dolomite with crystal size ranging from 25 to 50 μm. Notice microdolomite has been cross-cut by a micro-stylolite (Sty); c) Fabric preserving dolomite (Fpd) which is fine to medium crystalline planar-s dolomite; d) Fabric destructive dolomite (Fdd) which is medium to coarse crystalline planar-s dolomite with crystal size ranging from 100 to 150 μm. Crystals often have cloudy cores with clear rims. Fdd is crosscut by a low amplitude stylolite (Sty).

Figure 4. Photomicrographs of cathodoluminescence and BSE images showing the replacement dolomites (Md, Fpd and Fdd), dolomite cement (Cd), pyrite (Py), porosity (por.), mineral zonation (zone) and overgrowth rim of Fdd (rim): a) CL characteristics showing bright overgrowth rim of the fabric preserving dolomite (Fpd) and dolomite cement (Cd) and dark/non luminescent Fpd ; b) Porosity (Por) and pyrite minerals (Py) in the fabric preserving dolomite; c) CL characteristics showing dark/non luminescent microdolomite and bright dolomite cement (Cd) which occurred along the microstylolite; d) Polished section showing the porosity (Por) and pyrite minerals (Py) in the microdolomite; e) CL photomicrograph showing dull to slightly bright luminescent fabric destructive dolomite. Note the multi-zoned dolomite crystals; f) pore (Pore) and cubic pyrite (Py) in fabric destructive dolomite matrix.

Draft

Figure 5. Photomicrographs of paired cross-polarized and BSE images showing the dissolution of dolomite (Dis), cubic pyrite (Py) and quartz (Q): a) dissolution of Fdd and presence of cubic pyrite in vugs; b) microcrystalline quartz is observed in dissolution vugs of Fdd; c) the dissolution of Md along the stylolite developed in microdolomite and minor amount of microcrystalline quartz were filled in the dissolution vugs; d) microcrystalline quartz cement filling microporosity.

Figure 6. a) SEM image of fabric destructive, zoned dolomite crystal (Fdd). Dolomite crystal was analyzed along the line shown from core to overgrowth rim (EDS spot 1 to 16); b) Fe and Mn anomalies in overgrowth rims (EDS spot 15); c) very slight Fe and Mn anomalies in the core (EDS spot 10).

Figure 7. a) $^{87}Sr/^{86}Sr$ ratios versus numerical age for the replacement dolomites; $^{87}Sr/^{86}Sr$ curve is taken from Veizer et al., (1999). The top box shows the $^{87}Sr/^{86}Sr$ values of Eocene pluton (Karsli et al, 2007 and Eyuboglu, 2017). The bottom box represents the $^{87}Sr/^{86}Sr$ values of sandstone (McLennan at al., 1990). b) Cross-plots of $\delta^{18}O$ versus $\delta^{13}C$ of dolomite types. The blue box represents Upper Jurassic-Lower Cretaceous marine dolomite (Land, 1983; Veizer et al., 1999).

Figure 8. Cross-plots of Fe, Mn and Sr concentrations versus $CaCO_3$ for the replacement dolomites. The box represents marine dolomite (Vahrenkamp and Swart, 1990). A recrystallization and/or hydrothermal alteration trends are clear and distinct. The Fe and Mn concentrations are increased whereas Sr concentrations are decreased relatively the marine dolomites due to the epithermal vein polymetallic mineralization.

Figure 9. PAAS normalized REE pattern for fabric destructive dolomite (fdd): (a) Fabric preserving dolomite (b) and microdolomite (c) Cross-plots of Y/HO ratios versus La/Ho ratios. REE patterns of all types of dolomites distinct positive Eu (1.3 to 2.1) anomaly and

Draft

slightly flattened Ce anomalies (0.8 to 1.1). A recrystallization and/or hydrothermal alteration trend is apparent from Y/ Ho vs. La/Ho plot (Bau and Dulski, 1995).

Figure 10. Schematic model of the dolomitization (A) and recrystallization (B). With progressive burial, reactivation of extensional tectonics resulted in fracturing–faulting of the carbonate platform and formation of small-scale horst/graben system from time to time. Fractures could have provided suitable pathways for dolomitizing fluids of seawater origin and facilitated pervasive dolomitization of the formation. Fluid circulation and dolomite formation in response to the development of the fractures (A). Deeper burial processes, which occurred during Eocene magmatic event accompanied by hot hydrothermal fluids associated with emplacement of the polymetallic mineralization circulated in all dolomite and likely resulted in recrystallization and/or hydrothermal alteration of all types of dolomite. The alteration fluids may have interacted with overlying siliciclastics rocks to pick up a radiogenic signal during its infiltrating process (B).

Draft

950 **List of Tables**

951 **Table 1.** Summary of geochemical data obtained from replacement dolomites (Md, Fpd, Fdd)
952 and belemnites observed from the Berdiga Formation.

953 **Table 2.** Rare earth elements concentrations (REE+Y) of selected replacement dolomites
954 (Md, Fpd, Fdd) and belemnites (Blm) of the Berdiga Formation in Hazine Mağara area.

955

956

Draft

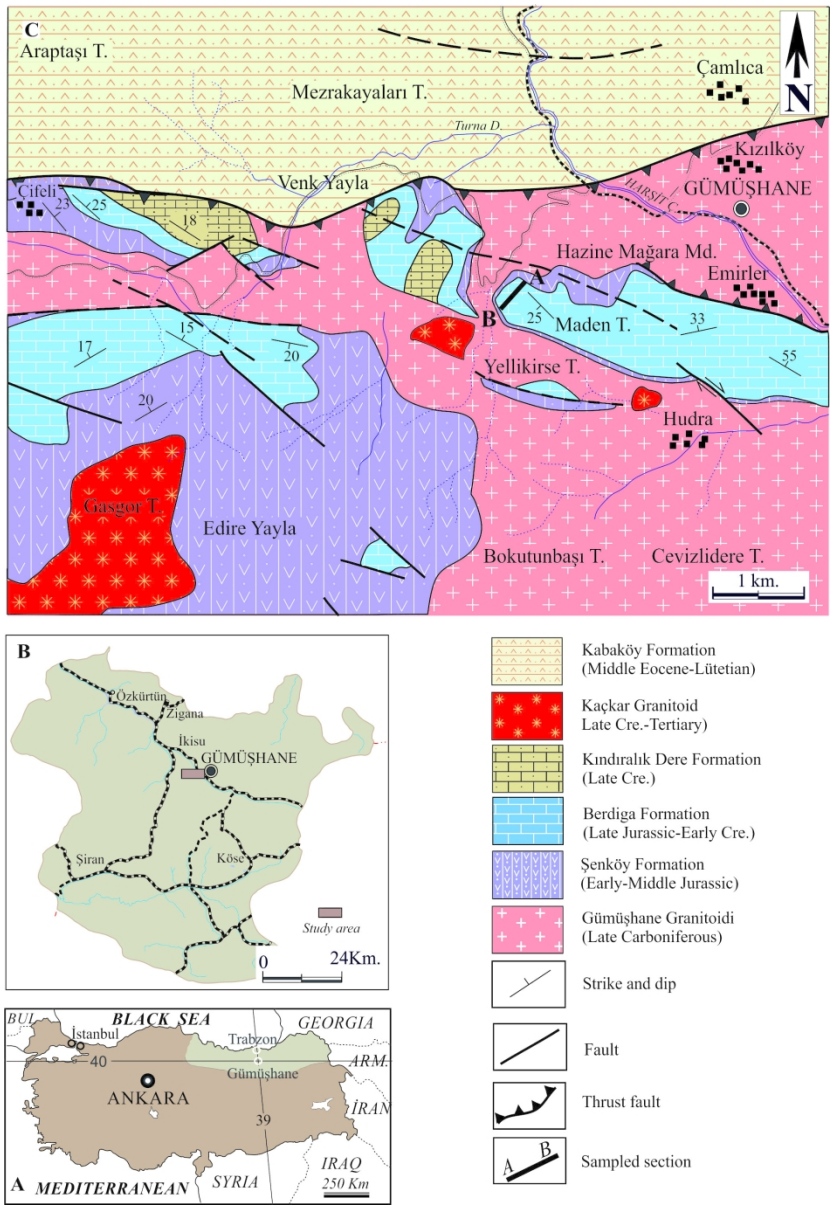
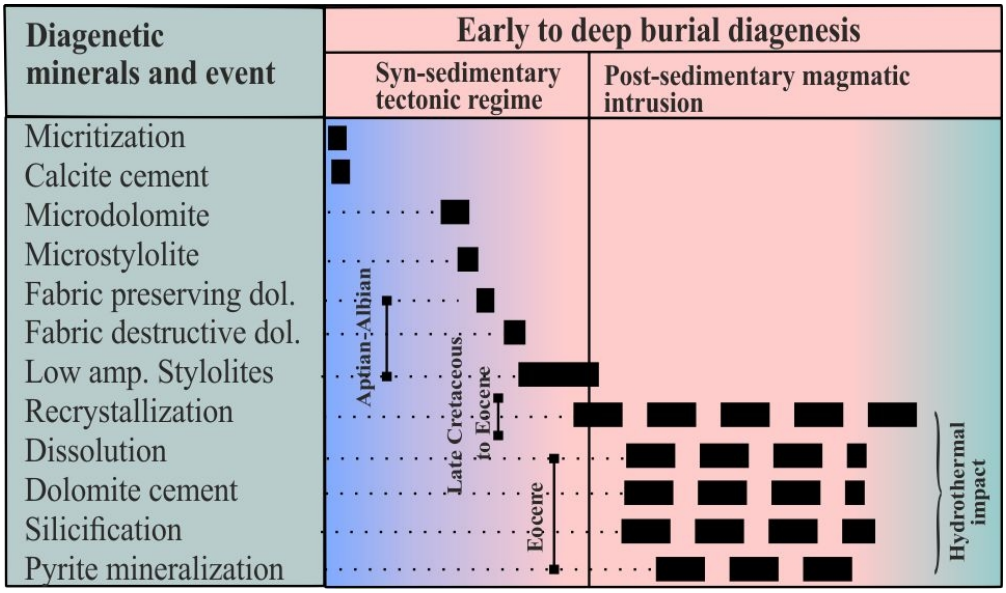


Figure 1. Location (A, B) and geological map of the study area (C) (modified after Güven, 1998).

174x253mm (300 x 300 DPI)



Paragenetic sequence of the studied formation showing early to late diagenetic processes.

81x47mm (300 x 300 DPI)

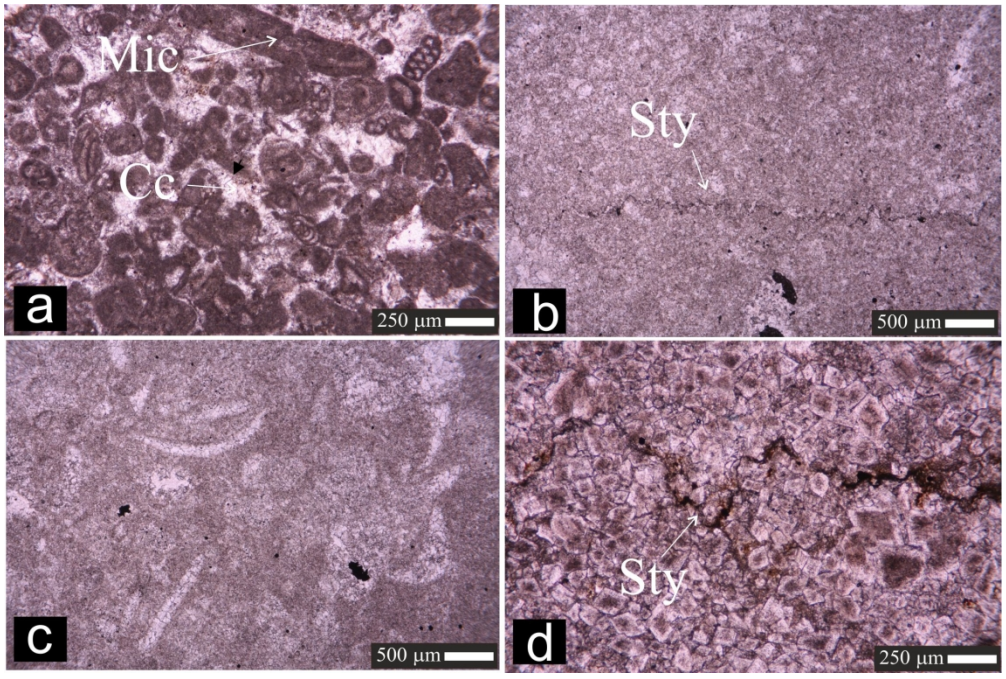


Figure 3. Photomicrographs of studied sections: a) grainstone facies. Mic: micritized allochem, Cc: Calcite cement; b) Microdolomite (Mc) which is microcrystalline planar-s dolomite with crystal size ranging from 25 to 50 µm. Notice microdolomite has been cross-cut by a micro-stylolite (Sty); c) Fabric preserving dolomite (Fpd) which is fine to medium crystalline planar-s dolomite; d) Fabric destructive dolomite (Fdd) which is medium to coarse crystalline planar-s dolomite with crystal size ranging from 100 to 150 µm. Crystals often have cloudy cores with clear rims. Fdd is crosscut by a low amplitude stylolite (Sty).

179x119mm (300 x 300 DPI)

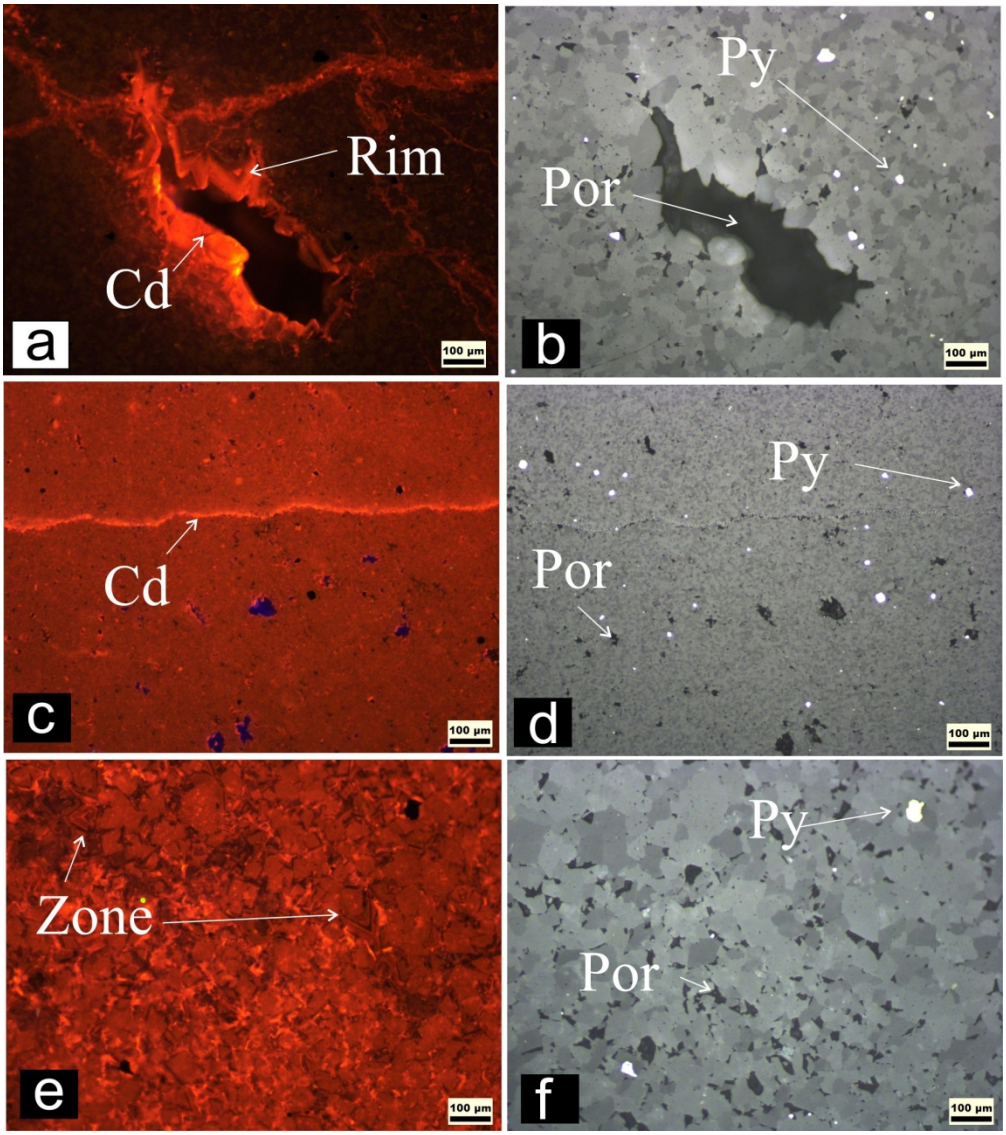


Figure 4. Photomicrographs of cathodoluminescence and BSE images showing the replacement dolomites (Md, Fpd and Fdd), dolomite cement (Cd), pyrite (Py), porosity (por), mineral zonation (zone) and overgrowth rim of Fdd (rim): a) CL characteristics showing bright overgrowth rim of the fabric preserving dolomite (Fpd) and dolomite cement (Cd) and dark/non luminescent Fpd ; b) Porosity (Por) and pyrite minerals (Py) in the fabric preserving dolomite; c) CL characteristics showing dark/non luminescent microdolomite and bright dolomite cement (Cd) which occurred along the microstylolite; d) Polished section showing the porosity (Por) and pyrite minerals (Py) in the microdolomite; e) CL photomicrograph showing dull to slightly bright luminescent fabric destructive dolomite. Note the multi-zoned dolomite crystals; f) pore (Pore) and cubic pyrite (Py) in fabric destructive dolomite matrix.

164x184mm (300 x 300 DPI)

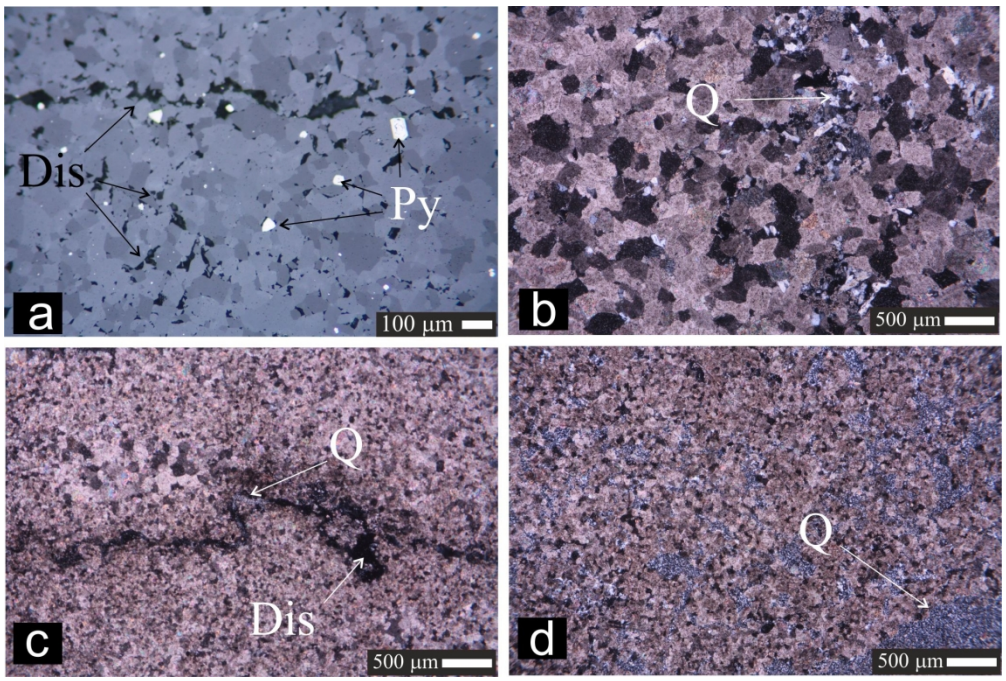


Figure 5. Photomicrographs of paired cross-polarized and BSE images showing the dissolution of dolomite (Dis), cubic pyrite (Py) and quartz (Q): a) dissolution of Fdd and presence of cubic pyrite in vugs; b) microcrystalline quartz is observed in dissolution vugs of Fdd; c) the dissolution of Md along the stylolite developed in microdolomite and minor amount of microcrystalline quartz were filled in the dissolution vugs; d) microcrystalline quartz cement filling microporosity.

176x118mm (300 x 300 DPI)

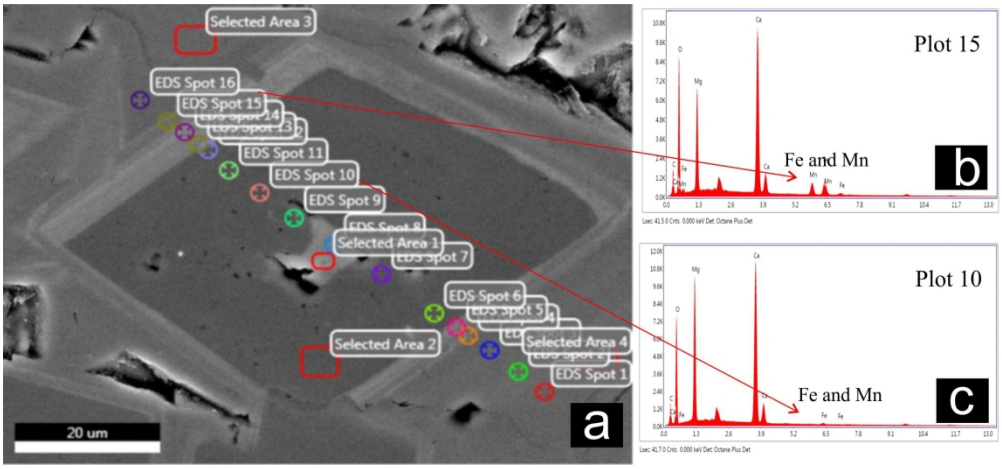


Figure 6. a) SEM image of fabric destructive, zoned dolomite crystal (Fdd). Dolomite crystal was analyzed along the line shown from core to overgrowth rim (EDS spot 1 to 16); b) Fe and Mn anomalies in overgrowth rims (EDS spot 15); c) very slight Fe and Mn anomalies in the core (EDS spot 10).

182x83mm (300 x 300 DPI)

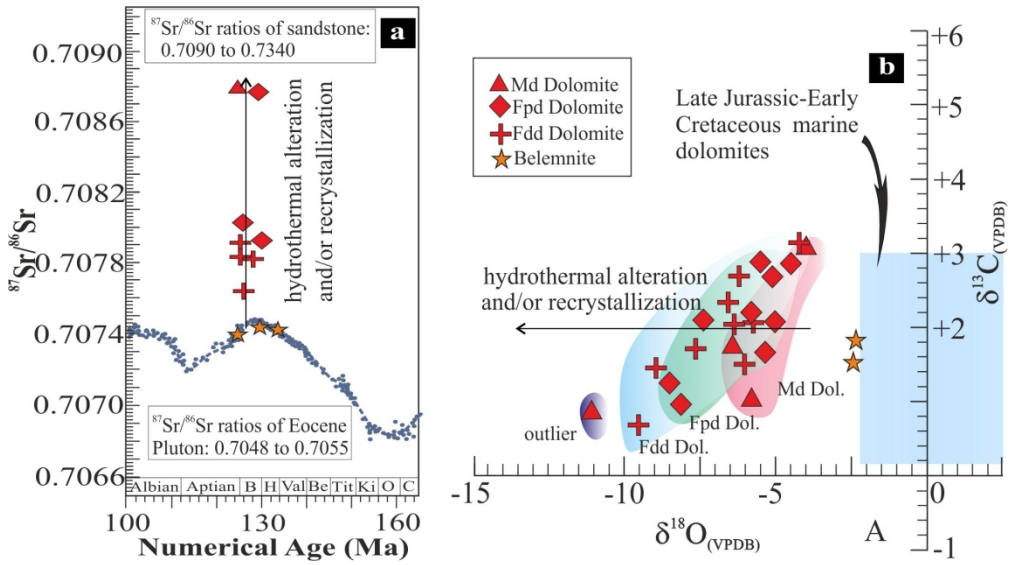


Figure 7. a) 87Sr/86Sr ratios versus numerical age for the replacement dolomites; 87Sr/86Sr curve is taken from Veizer et al., (1999). The top box shows the 87Sr/86Sr values of Eocene pluton (Karsli et al, 2007 and Eyuboğlu, 2017). The bottom box represents the 87Sr/86Sr values of sandstone (McLennan at al., 1990). b) Cross-plots of □18O versus □13C of dolomite types. The blue box represents late Jurrasic-early Cretaceous marine dolomite (Land, 1983; Veizer et al., 1999).

178x98mm (300 x 300 DPI)

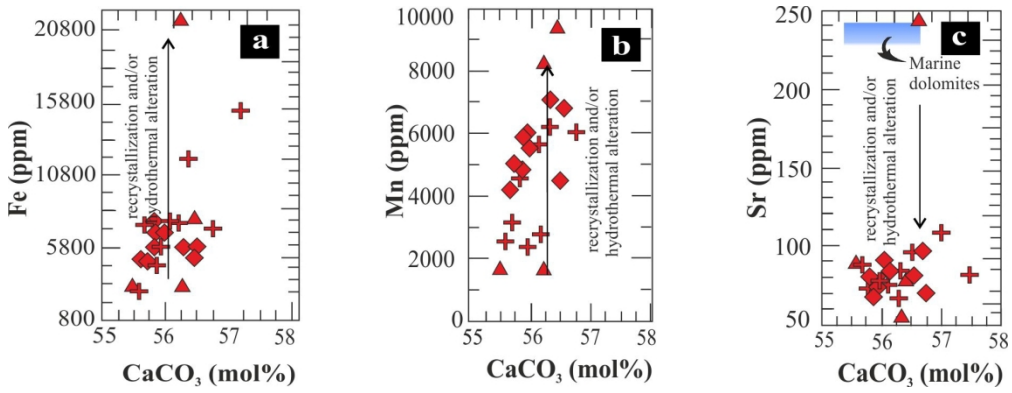


Figure 8. Cross-plots of Fe, Mn and Sr concentrations versus CaCO3 for the replacement dolomites. The box represents marine dolomite (Vahrenkamp and Swart, 1990). A recrystallization and/or hydrothermal alteration trends are clear and distinct. The Fe and Mn concentrations are increased whereas Sr concentrations are decreased relatively the marine dolomites due to the epithermal vein polymetallic mineralization.

158x60mm (300 x 300 DPI)

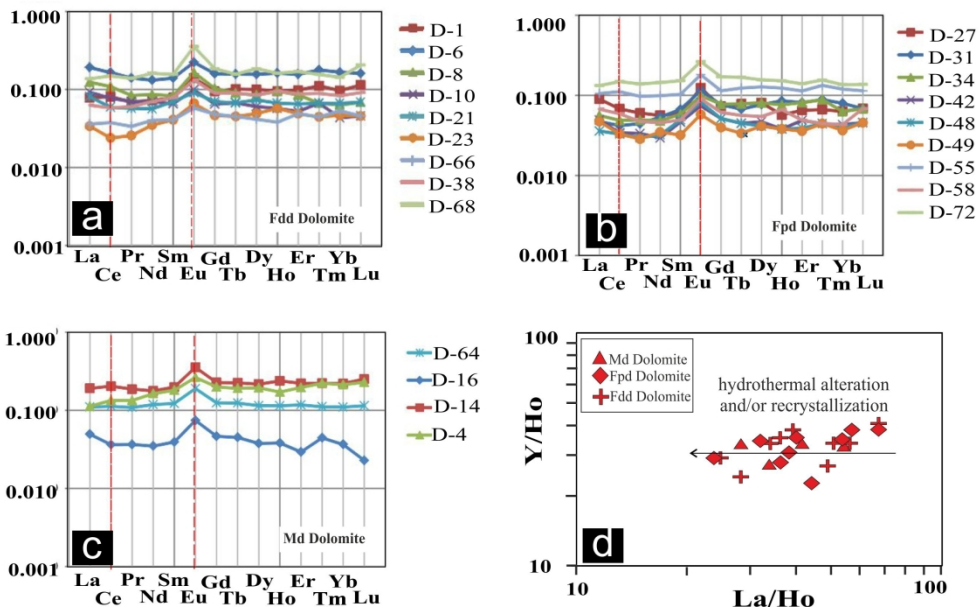


Figure 9. PAAS normalized REE pattern for fabric destructive dolomite (fdd): (a) Fabric preserving dolomite (b) and microdolomite (c) Cross-plots of Y/HO ratios versus La/Ho ratios. REE patterns of all types of dolomites distinct positive Eu (1.3 to 2.1) anomaly and slightly flattened Ce anomalies (0.8 to 1.1). A recrystallization and/or hydrothermal alteration trend is apparent from Y/ Ho vs. La/Ho plot (Bau and Dulski, 1995).

233x142mm (300 x 300 DPI)

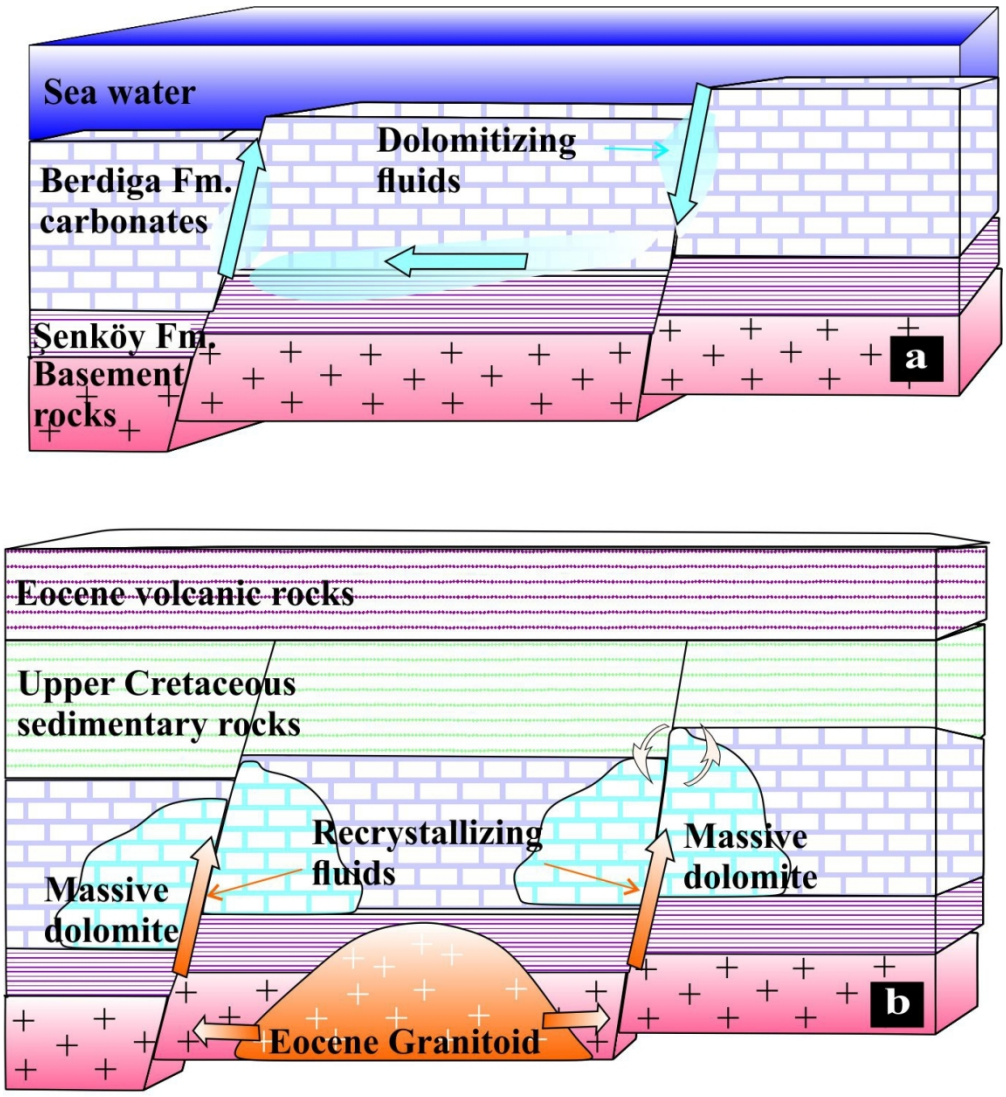


Figure 10. Schematic model of the dolomitization (A) and recrystallization (B). With progressive burial, reactivation of extensional tectonics resulted in fracturing–faulting of the carbonate platform and formation of small-scale horst/graben system from time to time. Fractures could have provided suitable pathways for dolomitizing fluids of seawater origin and facilitated pervasive dolomitization of the formation. Fluid circulation and dolomite formation in response to the development of the fractures (A). Deeper burial processes, which occurred during Eocene magmatic event accompanied by hot hydrothermal fluids associated with emplacement of the polymetallic mineralization circulated in all dolomite and likely resulted in recrystallization and/or hydrothermal alteration of all types of dolomite. The alteration fluids may have interacted with overlying siliciclastics rocks to pick up a radiogenic signal during its infiltrating process (B).

116x131mm (300 x 300 DPI)

Dolomite type/ Belemnite		$MgCO_3$ (mole %)	$CaCO_3$ (mole %)	Na (ppm)	Mn (ppm)	Fe (ppm)	Sr (ppm)	$\delta^{13}C$ (‰VPDB)	$\delta^{18}O$ (‰ VPDB)	$^{87}Sr/^{86}Sr$ (±2σ)
Md (n=4)	Max.	44	57	223	9294	21053	244	3.09	-4.05	0.70884
	Min.	43	56	74	1549	2728	56	0.86	-11.38	0.70884
	Avg.	44	56	167	5150	8621	117	1.68	-7.00	0.70884
Fpd (n=9)	Max.	44	57	223	7125	7554	97	2.93	-4.61	0.70879
	Min.	43	56	148	4337	4826	68	1.00	-8.73	0.70788
	Avg.	44	56	181	5585	5961	80	2.12	-6.32	0.70820
Fdd (n=9)	Max.	44	58	223	6196	15178	108	3.13	-4.14	0.70789
	Min.	42	56	74	2246	2798	67	0.69	-9.73	0.70753
	Avg.	44	56	140	4105	7772	83	1.99	-6.95	0.70774
Belemnite										
AF-7		1	99	742	bdl	560	1129	1.52	-2.51	0.70742
AF-13K		1	99	890	bdl	1049	989	1.84	-2.45	0.70742
AF-5		1	99	600	8	bdl	1038	0.10	-1.40	0.70741

Draft

		La (ppm)	Ce (ppm)	Pr (ppm)	Nd (ppm)	Sm (ppm)	Eu (ppm)	Gd (ppm)	Tb (ppm)	Dy (ppm)	Ho (ppm)	Er (ppm)	Tm (ppm)	Yb (ppm)	Lu (ppm)	Y (ppm)	ΣREE (ppm)
Md	D-4	5.00	11.80	1.35	6.10	1.24	0.32	1.20	0.17	1.03	0.18	0.60	0.10	0.64	0.10	5.90	29.83
Md	D-14	8.50	17.90	1.89	6.60	1.36	0.43	1.37	0.20	1.15	0.25	0.68	0.10	0.66	0.11	6.80	41.20
Md	D-16	2.20	3.20	0.37	1.30	0.27	0.09	0.28	0.04	0.20	0.04	0.09	0.02	0.11	0.01	1.30	8.22
Md	D-64	4.90	9.90	1.10	4.40	0.84	0.23	0.75	0.11	0.61	0.12	0.36	0.05	0.33	0.05	4.00	23.75
Fpd	D-27	4.00	6.00	0.61	2.10	0.41	0.15	0.44	0.07	0.43	0.06	0.20	0.03	0.19	0.03	2.30	14.72
Fpd	D-31	2.10	3.70	0.45	2.00	0.46	0.14	0.46	0.06	0.41	0.09	0.25	0.04	0.24	0.03	2.60	10.43
Fpd	D-34	2.50	4.30	0.50	1.80	0.40	0.12	0.47	0.07	0.43	0.08	0.25	0.04	0.19	0.03	2.70	11.18
Fpd	D-42	2.20	3.00	0.34	1.10	0.32	0.09	0.31	0.04	0.25	0.04	0.15	0.02	0.13	0.02	1.50	8.01
Fpd	D-48	1.60	2.90	0.30	1.20	0.34	0.10	0.31	0.04	0.22	0.04	0.12	0.02	0.12	0.02	1.40	7.33
Fpd	D-49	2.10	2.90	0.29	1.30	0.22	0.07	0.24	0.03	0.22	0.04	0.11	0.02	0.11	0.02	1.40	7.67
Fpd	D-55	4.70	9.80	0.99	3.70	0.71	0.22	0.69	0.11	0.68	0.13	0.35	0.06	0.36	0.05	3.70	22.55
Fpd	D-58	3.00	5.20	0.48	1.70	0.34	0.11	0.37	0.05	0.29	0.07	0.15	0.02	0.13	0.03	1.60	11.94
Fpd	D-72	5.90	13.10	1.41	5.40	1.05	0.32	1.03	0.15	0.83	0.16	0.43	0.07	0.41	0.06	4.90	30.32
Fdd	D-1	3.50	7.10	0.70	2.70	0.54	0.17	0.57	0.09	0.53	0.10	0.30	0.05	0.29	0.05	3.30	16.69
Fdd	D-6	8.50	14.50	1.42	4.90	0.96	0.27	0.96	0.14	0.83	0.17	0.48	0.08	0.50	0.07	4.60	33.78
Fdd	D-8	5.50	9.60	0.85	3.20	0.57	0.20	0.62	0.08	0.45	0.10	0.26	0.03	0.19	0.03	3.30	21.68
Fdd	D-10	4.10	6.80	0.71	2.60	0.45	0.12	0.39	0.06	0.32	0.06	0.16	0.03	0.13	0.02	2.40	15.95
Fdd	D-21	3.60	5.20	0.58	2.10	0.48	0.11	0.42	0.06	0.39	0.07	0.20	0.03	0.20	0.03	2.30	13.47
Fdd	D-23	1.50	2.10	0.26	1.30	0.28	0.08	0.28	0.04	0.26	0.06	0.15	0.02	0.14	0.02	1.70	6.49
Fdd	D-38	2.80	5.10	0.61	2.60	0.54	0.16	0.54	0.08	0.45	0.10	0.27	0.04	0.25	0.04	2.40	13.58
Fdd	D-66	1.60	3.30	0.34	1.50	0.28	0.07	0.29	0.04	0.22	0.04	0.15	0.02	0.16	0.02	1.50	8.03
Fdd	D-68	6.10	13.10	1.41	6.00	1.07	0.43	1.11	0.14	0.98	0.17	0.52	0.07	0.43	0.09	5.90	31.62
Blm	AF-7	<0.1	0.3	0.02	<0.3	<0.05	<0.02	<0.05	<0.01	<0.05	<0.02	<0.03	<0.01	<0.05	<0.01	0.1	0.42±0.3
Blm	AF-13K	<0.1	0.4	0.05	<0.3	<0.05	<0.02	0.05	<0.01	<0.05	<0.02	0.04	<0.01	<0.05	<0.01	0.3	0.84±0.3

Draft